

Nb-Ta-Sn Oxides From Lithium-Beryllium-Tantalum Pegmatite Deposits of the Kolmozero-Voronja Belt, NW Russia: Implications for Tracing Ore-Forming Processes and Mineralization Signatures

[Dmitry Zozulya](#)^{*}, Lyudmila Morozova, [Kåre Kullerød](#), Ayya Bazai

Posted Date: 7 November 2023

doi: 10.20944/preprints202311.0404.v1

Keywords: columbite group minerals; pyrochlore; cassiterite; pegmatite; lithium; beryllium; NW Russia



Preprints.org is a free multidiscipline platform providing preprint service that is dedicated to making early versions of research outputs permanently available and citable. Preprints posted at Preprints.org appear in Web of Science, Crossref, Google Scholar, Scilit, Europe PMC.

Copyright: This is an open access article distributed under the Creative Commons Attribution License which permits unrestricted use, distribution, and reproduction in any medium, provided the original work is properly cited.

Article

Nb-Ta-Sn Oxides from Lithium-Beryllium-Tantalum Pegmatite Deposits of the Kolmozero-Voronja Belt, NW Russia: Implications for Tracing Ore-Forming Processes and Mineralization Signatures

Dmitry Zozulya ^{1,*}, Lyudmila Morozova ^{1,2}, Kåre Kullerød ³ and Ayya Bazai ¹

¹ Geological Institute of the Kola Science Centre of the Russian Academy of Sciences, 14 Fersman St., 184209 Apatity, Russia

² All-Russian Scientific-Research Institute of Mineral Resources Named after N.M. Fedorov, 31 Staromonetny Ln, 119017 Moscow, Russia

³ Norwegian Mining Museum, Hyttegata 3, 3616 Kongsberg, Norway

* Correspondence: zozulya@geoksc.apatity.ru

Abstract: In this paper we present textural and compositional data for columbite group minerals (CGM) and associated Nb-Ta-Sn oxides from lithium-beryllium-tantalum pegmatite deposits of the Kolmozero-Voronja belt, NW Russia, with the aim of deciphering the above mentioned features for minerals from deposits with different mineral signatures and lithium ore grade. Minerals from four deposits, including two of world-class (Kolmozero and Polmostundra), are examined. It is shown that the main controlling factors are the diversity and rate of magmatic fractionation, hydrothermal overprint and mineral paragenesis followed from the specific geochemical signature of the different pegmatite deposits. CGM from Kolmozero include several mineral species (columbite-(Fe), columbite-(Mn), tantalite-(Fe), tantalite-(Mn)) showing large compositional variations, mainly controlled by Nb-Ta fractionation ($Ta/(Ta+Nb) = 0.16-0.70$; $Mn/(Mn + Fe) = 0.45-0.63$). Textural patterns are extremely various (oscillatory, homogeneous, patchy, spongy, somewhere with overgrowing Ta-rich rims) and indicate the involvement of numerous magmatic and hydrothermal processes. The Polmostundra CGM are represented by columbite-(Fe) with $Ta/(Ta+Nb)$ ranging from 0.05 to 0.39 with homogeneous, mottled, oscillatory, patchy and irregular reverse textures. The Okhmylk CGM are irregular normal, patchy and homogeneous columbite-(Fe) and columbite-(Mn) with $Ta/(Ta+Nb) = 0.09-0.24$ and $Mn/(Mn + Fe) = 0.29-0.92$, indicating the suppressed magmatic fractionation and iron drop due to precipitation of Fe minerals. Columbite-(Fe) and columbite-(Mn) from the Be-Ta Shongui deposit are less evolved with $Ta/(Ta+Nb) = 0.07-0.23$ and $Mn/(Mn + Fe) = 0.31-0.55$. The minerals are characterized by progressive normal, oscillatory, homogeneous and irregular reverse patterns. Associated pyrochlore minerals occur both as early magmatic (Kolmozero) and late hydrothermal (Polmostundra, Okhmylk). Cassiterite is found only in the Okhmylk dykes and is apparently of hydrothermal origin. CGM from Li pegmatites have impurities of Ti (0.01-0.05 apfu) and W (up to 0.02 apfu), whereas CGM from Be pegmatites contains elevated Ti (up to 0.09 apfu). The mineral systems analysis presented here is relevant for exploration.

Keywords: columbite group minerals; pyrochlore; cassiterite; pegmatite; lithium; beryllium; NW Russia

1. Introduction

Columbite-group minerals (CGM) with ideal formula AB_2O_6 ($A = Mn, Fe$; $B = Nb, Ta$) are important accessory minerals in granitic pegmatites, and constitute the principal Nb-Ta ore minerals in rare-element pegmatite dykes of the LCT (lithium-cesium-tantalum) petrogenetic family (e.g. [1–9]). The CGM record ore-forming processes due to their common occurrence in most pegmatite zones coupled with complex internal structures and compositional variations in Nb/Ta and Fe/Mn (e.g.

[6,10–17]). In general, columbite - tantalite compositions exhibit enrichment in Mn and Ta with progressive fractionation of granitic-pegmatite-forming melt – fluid systems [1,2,18,19]. In certain Li-rich pegmatites, the composition of columbite - tantalite evolved extensively from columbite-(Fe) to tantalite-(Mn), suggesting the involvement of hydrothermal processes and that the activity of F increased substantially during crystallization [19,20].

The occurrence of CGM together with other Nb-Ta oxides (e.g. pyrochlore and wodginite group minerals) has attracted significant attention because they are minerals of economic interest for Ta, hosted in several high-grade deposits worldwide [14,15,18,21]. In general, the Nb-Ta oxide mineral assemblage changes from columbite - tantalite + ixiolite to columbite - tantalite + microlite + ixiolite + cassiterite + wodginite to microlite + columbite-(Mn) with increasing fractionation.

In this paper, we focus on the internal zoning pattern and major-element composition of CGM and associated Nb-Ta-Sn oxides in pegmatites from four Li-Be-Ta deposits of the Kolmozero-Voronja zone (Kola region, NW Russia), including two of world-class, with the aim of revealing the evolutionary history of the Li-rich pegmatite and deciphering the relationship between pegmatites of different mineralization signatures and ore grade.

2. Geology of the Kola rare-metal pegmatite belt

The Kola rare-metal pegmatite belt is located in the northeastern part of the Fennoscandian shield in the Kola region and extends from the Lake Kolmozero to the northwest, almost to the border with Norway. It has a length of more than 300 km and a width of 20 to 45 km. The belt contains up to 95% of granitic pegmatite dikes with rare-metal mineralization (Be, Ta, Nb, Cs, Li) found on the Kola Peninsula [22]. There are six deposits of rare-metal pegmatites within the pegmatite belt. The Polmostundra, Oleniy Ridge, Vasin-Mylk and Okhmylk deposits are confined to the Kolmozero-Voronja greenstone belt. The Kolmozero field is located in the Murmansk province, and the Shongui field is located in the Kola province (Figure 1).

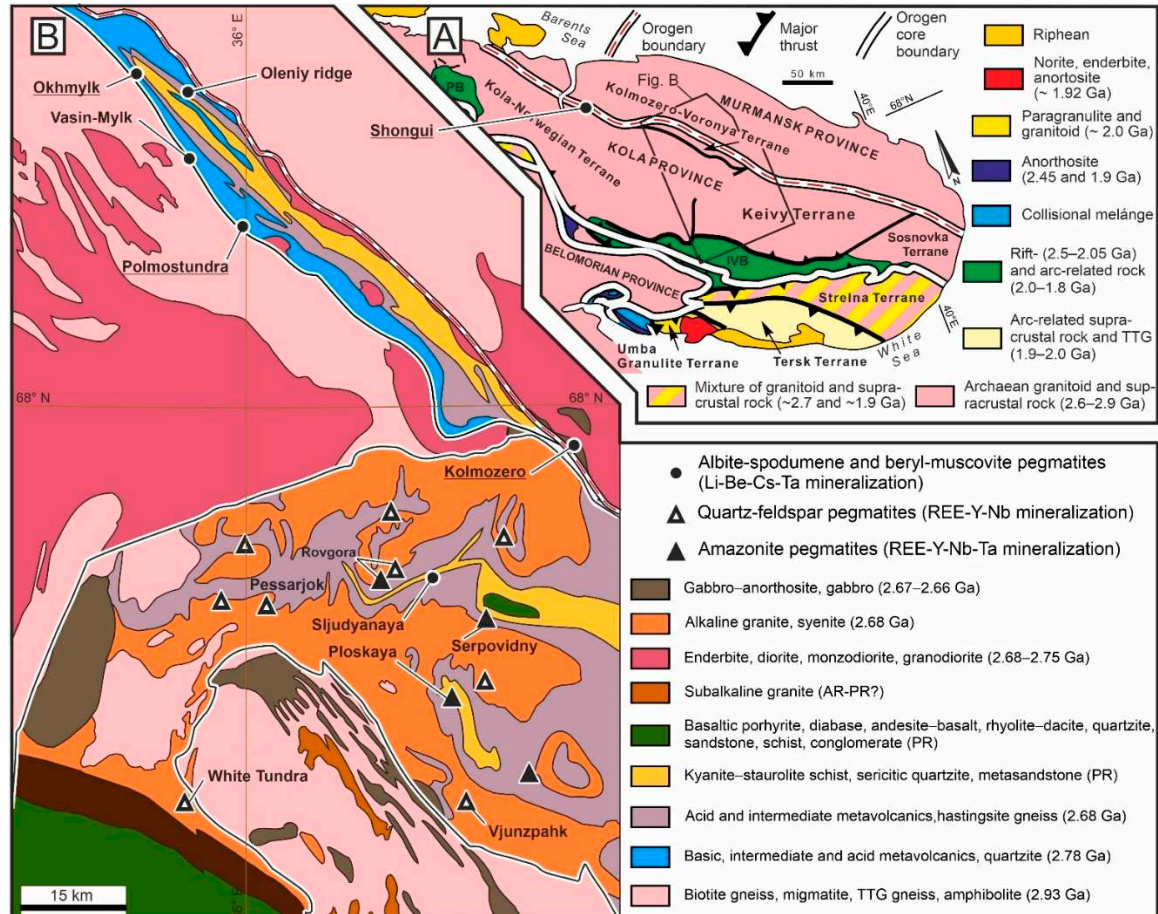


Figure 1. (A) - main geological units of the NE Fennoscandian Shield. (B) - simplified geological map of the Kola rare-metal pegmatite belt with location of deposits (in addition the Keivy REE-Zr-Nb-Ta pegmatite deposits are shown (see description in [33]). The studied deposits are underlined.

The Murmansk province is dominated by Late Mesoarchean and Neoarchean granites, enderbites, charnockites, and tonalite-trondhjemite gneisses with relics of supracrustal formations. These rocks were metamorphosed under conditions of high-temperature amphibolite facies and locally contain relics of granulite facies mineral parageneses [23].

The main tectonic units of the Kola Province are the Kola-Norwegian, Keivsky, and Kolmozero-Voronya terranes [24]. The Kola-Norwegian and Keivy terranes are mainly composed of tonalite-trondhjemite-granodiorite gneisses, charnockites and enderbites, metasediments and subordinate amphibolites.

The Kolmozero-Voronya greenstone belt, which was formed 2.92–2.79 Ga ago, is composed of the Polmos-Poros rocks series, represented by four formations (from bottom to top): Lyavozero (lower terrigenous sequence), Polmostundra (komatiite-tholeiite series), Voronietundra (basalt-andesite-dacite series) and Chervutskaya (upper terrigenous sequence). Greenstone rocks were metamorphosed under amphibolite facies conditions [25–27]. The continental crust of the Murmansk and Kola provinces was formed and underwent significant metamorphic and deformational reworking 2.6–2.9 Ga ago [28].

The main tectonic boundaries of northern Fennoscandia were finally formed in the Paleoproterozoic during the Lapland–Kola collisional orogeny [24,28]. The history of the Lapland–Kola collisional orogen includes intracontinental rifting of the Archean crust (2.5–2.1 Ga), rift opening (~2.1–2.0 Ga), subduction and crustal growth (~2.0–1.9 Ga) intercontinental collision (1.94–1.86 Ga), and orogenic collapse and exhumation (1.90–1.86 Ga). The Kola Province was the northeastern part of the Lapland–Kola Orogen and underwent Paleoproterozoic deformational reworking mainly along the boundaries of the main tectonic structures, while the Murmansk Province was practically not affected by Paleoproterozoic deformation [24].

The Kola rare-metal pegmatite belt spatially coincides with the junction zone of the Archean Murmansk and Kola provinces. This junction zone was considered for a long time as an Archean linear mobile-permeable zone (deep fault), which was partially activated in the Paleoproterozoic and is now interpreted as the Kolmozero-Voronya Archean collisional suture [23]. This suture is bordered and penetrated by zones of highly deformed rocks, which are considered to be transcrustal shear zones. Due to their high permeability, these zones were channels through which ore-bearing fluids could circulate. Ore components were deposited both inside the zones, but also in the surrounding rocks [29]. The Kolmozero and Polmostundra deposits include albite-spodumene type pegmatites, containing about 20 volume percent spodumene [30–32]. The Vasin-Mylk and Okhmylk deposits are complex and contain the lithium ore minerals spodumene and lepidolite, and the cesium mineral pollucite. The pegmatites of the Shongui deposit are of the beryl type, containing beryl as an accessory ore mineral. For all of the above-mentioned deposits, columbite group minerals occur as accessory minerals, and are of commercial interest due to the large volumes of the pegmatite ores.

The Kolmozero deposit includes 12 large albite-spodumene pegmatite dykes more than 1400 m long, from 5 to 65 m thick, and are documented to a depth of more than 500 m. The pegmatite dikes are tabular-shaped and do not show any pronounced concentric zonation. Quartz-plagioclase aplite up to 5 cm thick and coarse-grained quartz-albite aggregates up to 30 cm thick are observed at the contact with the host rocks. The main part of the dikes (85–90%) is almost composed of coarse-grained quartz-spodumene-feldspar pegmatite. Some domains are composed of a quartz-spodumene aggregate of a coarse-grained structure. The main minerals of the pegmatite are: quartz (30–35 vol.%), albite (30–35 vol.%), microcline (10–25% vol.%), spodumene, that is the main lithium mineral (~20% vol.%), and muscovite (5–7 vol.%). Accessory minerals include spessartine, apatite, beryl, columbite group minerals, and accessory lithiophyllite, triphylite and tourmaline. In total, 64 mineral species have been identified in the pegmatites of the Kolmozero lithium deposit [34]. Columbite-(Mn) from the albite-spodumene pegmatite has yielded a U-Pb age of 2315 ± 10 Ma, which is interpreted as the

age of the rare-metal mineralization [35]. This age indicates that the albite-spodumene pegmatites were formed during the Early Paleoproterozoic rifting of the Fennoscandian Shield [36].

The *Polmostundra deposit* is composed of five tabular-shaped albite-spodumene pegmatite dikes occurring in amphibolites of the Polmostundrovskaya suite of the Kolmozero-Voronya greenstone belt. The pegmatite dikes are 1000–1300 m long, up to 40 m thick, and explored to depths of up to 200–300 m. In general, the margins of the pegmatite are composed of granite pegmatite, while aplite occurs along the footwall, however, along strike and toward depth both mineralogy and textures show variations. The major minerals of the Polmostundra pegmatites are quartz (30–50 vol.%), albite (10–70 vol.%), spodumene (5–50 vol.%), and microcline (up to 20 vol.%). Minor and accessory minerals include muscovite, tourmaline, garnet, apatite, columbite group minerals and beryl. More rare minerals include zeolites, vivianite, sulfides, carbonates, lithiophyllite and eucryptite. Holmquistite, biotite, magnetite and epidote group minerals can be observed along the contact with the host amphibolites [22].

The *Okhmylk deposit* is composed of pegmatite dykes of various thicknesses and lengths, occurring in amphibolites of the Polmostundra Formation of the Kolmozero-Voronya greenstone belt. The length of the dikes varies from 25 to 700 m, and the thickness varies from a few meters to 45 m. The pegmatite dikes show an internal mineralogical and textural zonation. The 0.4 to 4 m thick marginal part of the dikes (zone 1) at the contact with amphibolite is composed of an aggregate of quartz and feldspar. Minor and accessory minerals include muscovite, black tourmaline, garnet, magnetite and apatite. Towards the center of the dikes, zone 2 is represented by an aggregate of quartz and feldspar together with columbite group minerals, beryl, garnet, aggregates of apatite and isolated spodumene crystals. Zone 3 is composed of a quartz-albite-spodumene aggregate. The main minerals are quartz (60 – 65 vol.%), spodumene (~20 vol.%) and albite (10 – 15 vol.%). Minor and accessory minerals include tourmaline, beryl, columbite group minerals and microcline. Zone 4 is characterized by blocky quartz and microcline. The major minerals include microcline (60 – 70 vol.%), quartz (15 – 25 vol.%) and albite (5 – 15 vol.%). Minor and accessory minerals are spodumene (up to 5%), polychrome tourmaline, lepidolite, pollucite, muscovite, columbite group minerals, lithiophyllite and montebrasite. Recent U-Pb (SHRIMP-RG) geochronological data of zircon from the Okhmylk pegmatite dyke yielded an age of 2607 ± 9 Ma [37]. We consider this age as the most reliable for the formation of the Li-Cs-Ta pegmatite deposits of the Kolmozero-Voronya belt.

The *Shongui deposit* consists of three 400 to 1000 m long and 60 to 80 m thick pegmatite dikes. The host rocks are amphibolites of the Kola province. The main rock-forming minerals of the dikes are quartz (30–35 vol.%), plagioclase (30–35 vol.%) and microcline (20–25 vol.%). Accessory minerals include beryl, spodumene, columbite group minerals, tourmaline, muscovite, garnet, zircon, apatite, molybdenite, pyrite, arsenopyrite and ilmenite. About 5 m thick quartz-albite and quartz-microcline-albite aggregates occur along the margins of the pegmatite dikes, in contact with the host amphibolites. The major volume of the dikes (75–80%) is composed of quartz-microcline and quartz-microcline-albite aggregates, including domains of quartz-clevelandite and albite-muscovite-quartz aggregates [38]. The only a geochronological determination known from the Shongui pegmatites, was performed by the K-Ar method on micas, which gave an age of 2.35–2.10 Ma [39].

Sampled pegmatites from the Kolmozero-Voronya area (i.e., those with economic potential, including the Kolmozero lithium deposit, the Polmostundra lithium-caesium deposit, the Okhmylk lithium deposit and the Shongui beryllium deposit) belong to the LCT petrogenetic family, rare element class, spodumene and beryl-columbite subtypes (according to the classification of [40]). As no relationships between the studied pegmatites and the pronounced S-type granitic bodies in region have been established, the anatectic model rather than the differentiation model can be applied to explain the formation of these fields. According to the anatectic model, pegmatites are considered to have formed from melts produced by partial melting of suitable lithologies, usually pelitic metasediments and/or metavolcanics (e.g., [41,42,43]).

3. Methods and sampling

The studied pegmatite samples (10-12 kg) were collected from typical rare-element pegmatite dykes (coarse-grained parts) from the Kolmozero-Voronja deposits, which mainly consist of quartz, albite, K-feldspar and spodumene, with minor and accessory muscovite, tourmaline and garnet (Table 1). Based on the Li₂O content, sample KL-GX-11 from Kolmozero classifies as high-grade (> 1.5 wt. % Li₂O), sample POL-GX-3/5 from Polmostundra as medium- to low-grade (0.4-1.5 wt. %), while sample OKH-2/2 from Okhmylk classifies as low-grade to barren (<0.4 wt. %). Sample SH-7 from Shongui, which consists mainly of quartz and albite, with minor and accessory beryl, tourmaline, apatite and garnet, shows only traces of Li₂O. The whole rock chemistry is in accordance with the mineral contents of the samples (Table 1).

Table 1. Mineralogical and geochemical characterization of the studied samples.

Deposit/Occurrence	Kolmozero	Polmostundra	Okhmylk	Shongui
Sample N	KL-GX-11	POL-GX-3/5	OKH-2/2	SH-7
Major and minor minerals	quartz, 50-60 %; feldspar (microcline + albite), 20-25 %; spodumene, 20%	quartz, 50-60 %; feldspar (microcline + albite), 25-30%; lepidolite, 10%; spodumene, 3%	quartz, 50-60 %; feldspar (microcline + albite), 40-45 %; tourmaline (mainly schorl), 3%; spodumene, 1%	quartz, 60-65%; feldspar (mainly albite), 35-40%
Accessory minerals	garnet, apatite, magnetite, ilmenite	apatite, tourmaline, garnet, magnetite, rutile, ilmenite	apatite, magnetite, garnet	beryl, tourmaline, apatite, garnet, magnetite,
Nb-Ta-Sn oxides	CGM	CGM, pyrochlore/microlite	CGM, pyrochlore, cassiterite	CGM, pyrochlore
Wet chemistry (wt.%)				
SiO ₂	75.52	75.08	76.10	85.33
TiO ₂	<0.01	<0.01	0.03	0.02
Al ₂ O ₃	14.81	12.75	12.10	7.33
Fe ₂ O ₃	0	0.11	0.00	0.09
FeO	2.69	1.89	1.57	1.67
MnO	0.11	0.065	0.04	0.18
MgO	0.17	0.08	0.12	0.24
CaO	0.1	0.11	0.23	0.20
Na ₂ O	2.48	3.59	6.11	4.15
K ₂ O	1.25	3.5	2.40	0.17
Li ₂ O	2.27	0.55	0.138	0.005
CO ₂	0.25	0.02	<0.1	<0.1
F	0.014	0.32	0.017	0.007
Cl	0.005	0.005	0.007	0.011
P ₂ O ₅	0.08	0.34	0.13	0.10
ICP-MS (ppm)				
Li	11000	2200	800	29
Be	100	13	7	27
Rb	500	4300	600	11
Nb	49	50	80	23
Sn	30	31	4	1,8
Cs	30	2200	70	17
Ta	17	160	18	8.5
W	1.2	24	1.4	0.3

Note. Wet chemistry analyses (for major elements by atomic absorption spectrophotometry; TiO₂ by colorimetry; K₂O, Na₂O and Li₂O by flame photometry; FeO and CO₂ by titration; and F and Cl by potentiometry using an ion-selective electrode) were performed in Geological Institute, Kola Science Centre RAS, Apatity. ICP-MS data were obtained from Analytical Centre "Geoanalyst" (Zavaritsky Institute of Geology and Geochemistry of the Ural Branch RAS).

Although CGM and other Nb-Ta-Sn oxide grains were not directly observed within polished thin sections and hand specimens, the minerals were successfully separated from about 500 g crushed samples using heavy liquid and magnetic separator and by hand-picking under a binocular microscope. Fifteen to 25 grains of CGM from each sample were mounted in epoxy resin and polished by standard methods. As shown in Figures 2–5, the examined CGM grains are anhedral to subhedral fragments of isometric (rarely elongated) shape. The size of the grains varies from 300 to 600 μm .

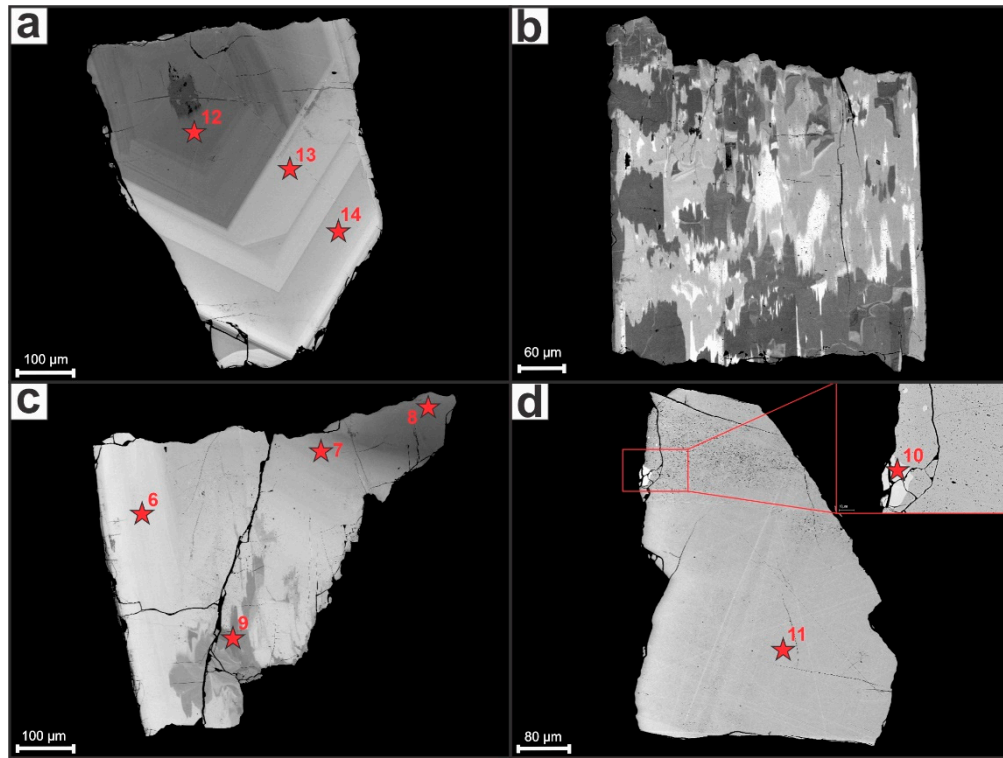


Figure 2. Representative back-scattered electron (BSE) images of CGM grains from the Kolmozero pegmatites, illustrating the internal textures. CGM with normal oscillatory (a), patchy (b), reverse irregular (c) zoning/pattern and homogeneous grain (d). Inclusion of rectangular Nb-Ta-Ca-Na-oxide in (a) and porous parts (d). The numbered red stars indicate points analyzed by microprobe - the numbers (in Figures 2–10) refer to analyses given in Tables 2–4 and Supplementary materials.

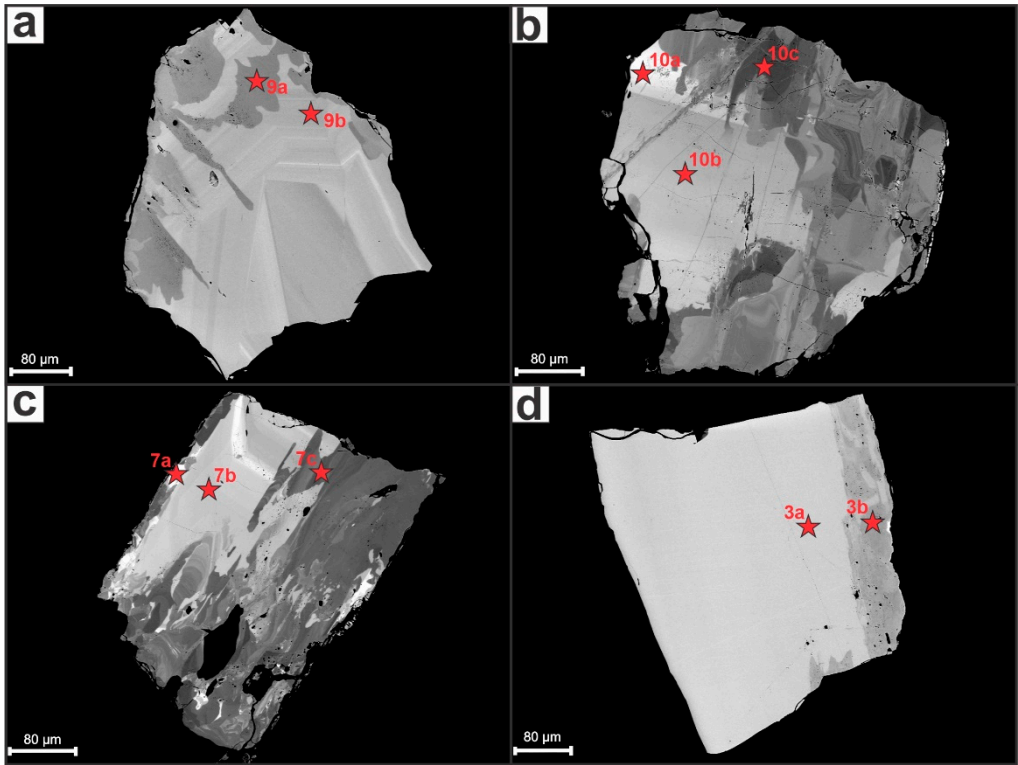


Figure 3. Representative back-scattered electron (BSE) images of CGM grains from the Polmostundra pegmatites, illustrating the internal textures. CGM with mottled (a, b), patchy (c), zoning and homogeneous grain with BSE-lower and porous rim (d). Internal remnants of CGM with oscillatory (a) and homogeneous (b) textures.

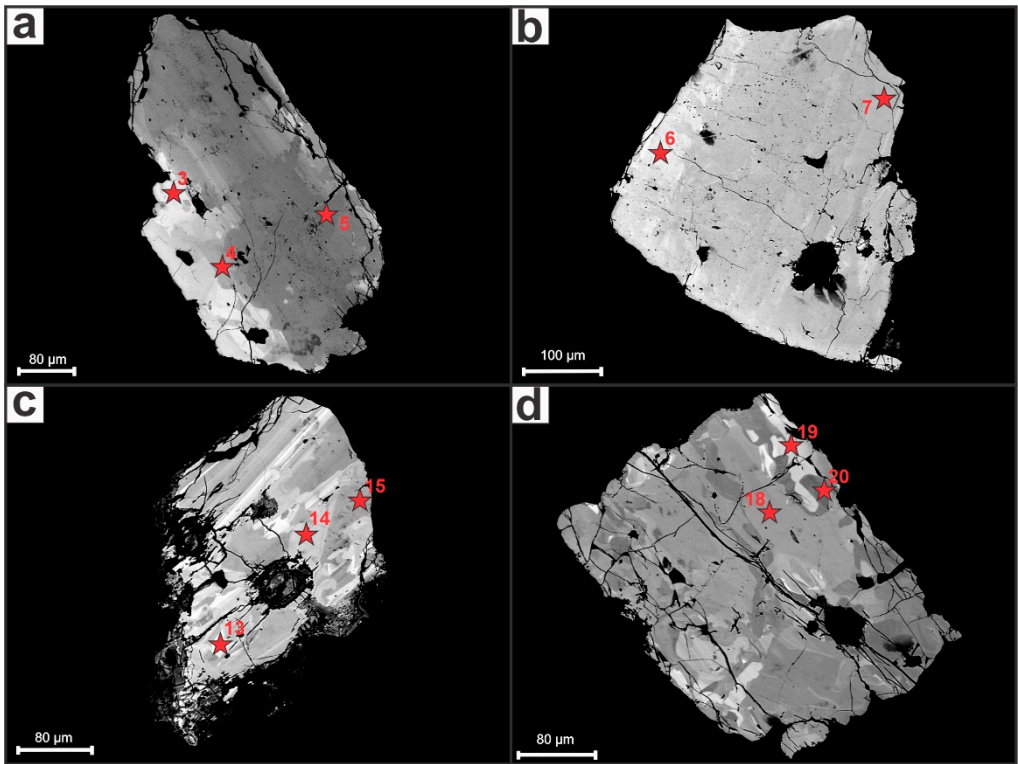


Figure 4. Representative back-scattered electron (BSE) images of CGM grains from the Okhmylk pegmatites, showing variations in the internal textures. CGM with normal irregular zoning (a, b) and patchy pattern (c, d).

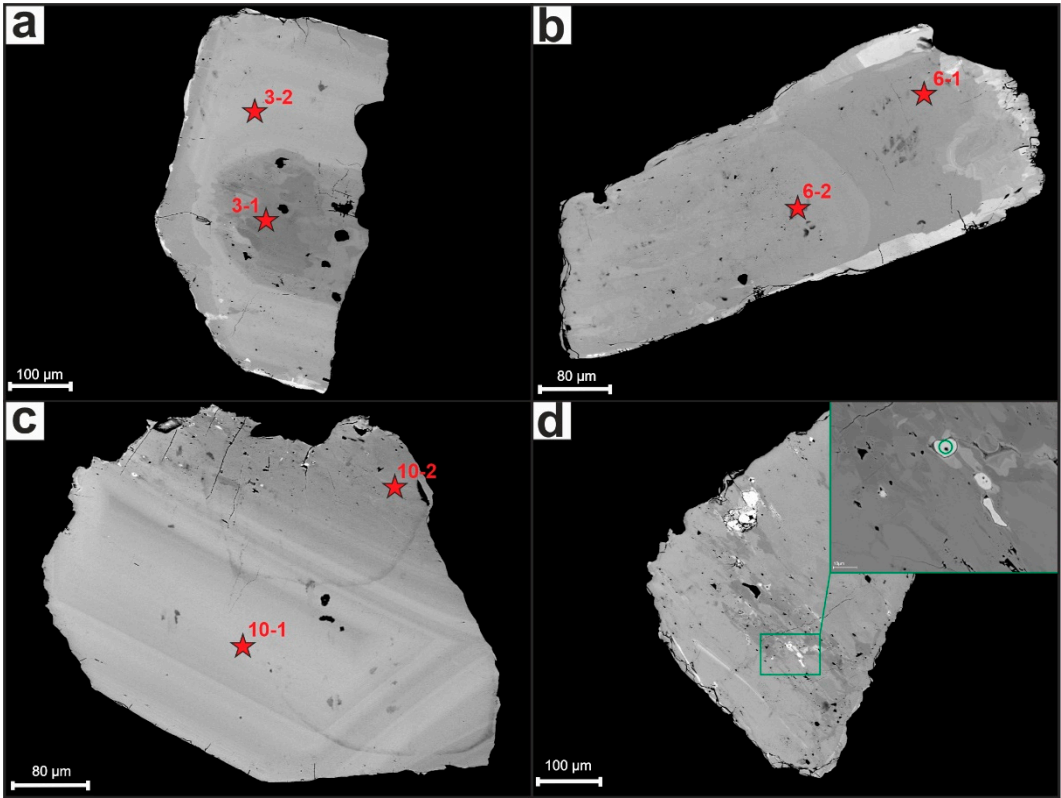


Figure 5. Representative back-scattered electron (BSE) images of CGM grains from the Shongui pegmatites, illustrating the internal textures. CGM with normal irregular (a) homogeneous with bright thin rims (b), transition of oscillatory to homogeneous zoning (c) and homogeneous grain with darker core (d). Inclusions of Ta-Nb-Ca-Si-Ti(±Sn) oxide (d).

Initially, the sample preparates were studied under a Leo-1450 electron microscope with an OXFORD ULTIM MAX 100 energy dispersive microanalyzer and AZtec software (including elements from C to U). Precise determination of the composition (including elements from Na to U) of all the phases detected under the initial study was carried out using a Cameca MS-46 wave-dispersive electron probe microanalyzer with a probe current of 20–30 nA, an accelerating voltage of 20 kV, and a probe diameter of 5–10 µm. The following natural minerals were used as standards: lorenzenite (Na, Ti), pyrope (Mg, Al), diopside (Si, Ca), fluorapatite (P), barite (S and Ba), atacamite (Cl), wadeite (K), tortveitite (Sc), hematite (Fe), chromite (Cr), celestine (Sr), thorite (Th), lepidolite (Rb), pollucite (Cs), cassiterite (Sn) and uraninite (U). In addition, the following synthetic standards were used: Y₂Al₅O₁₂ (Y), MnCO₃ (Mn), ZnO (Zn), NiAs (As), ZrSiO₄ (Zr), PbTe (Te), LaCeS₂ (La, Ce), LiPr(WO₄)₂ (Pr), LiNd(MoO₄)₂ (Nd), LiSm(MoO₄)₂ (Sm), LiEu(MoO₄)₂ (Eu), LiGd(MoO₄)₂ (Gd), LiDy(WO₄)₂ (Dy), PbSe (Pb), and metallic vanadium, cobalt, nickel, copper, hafnium, niobium, tantalum, molybdenum, palladium, platinum, gold, silver, bismuth, antimony and tungsten.

A total of 102 compositions of Nb-Ta-Sn oxides were obtained by electron probe microanalyzer. Representative chemical analyzes of CGM, pyrochlore super-group minerals (PSGM) and cassiterite are given in Tables 2–4; whole data set (including relevant BSE images) is given in Supplementary materials.

Table 2. Representative compositions of CGM from the Kolmozero, Polmostundra, Okhmylk and Shongui pegmatites.

Kolmozero											
Sample #	6	7	8	9	10	11	12	13	14	19	20
MgO	0.07	0.06	0.05	0.00	0.06	0.00	0.00	0.00	0.07	0.00	0.00
Al ₂ O ₃	0.00	0.00	0.00	0.00	0.00	0.07	0.00	0.00	0.00	0.00	0.00

SiO ₂	0.79	0.61	0.36	0.52	1.40	0.92	0.25	0.47	0.39	0.17	0.22
CaO	0.06	0.05	0.05	0.05	0.14	0.05	0.19	0.09	0.04	0.00	0.00
TiO ₂	0.75	0.60	0.46	0.48	0.90	0.78	0.49	0.46	0.47	0.29	0.44
V ₂ O ₅	0.00	0.00	0.00	0.00	0.00	0.00	0.00	0.00	0.00	0.07	0.08
MnO	7.44	7.79	8.66	8.45	2.78	8.18	8.54	11.20	7.98	11.11	11.08
FeO	8.94	9.45	10.37	9.57	12.30	7.87	10.28	9.46	10.00	8.43	8.54
ZnO	0.17	0.12	0.07	0.13	0.13	0.20	0.00	0.11	0.13	0.00	0.00
ZrO ₂	0.00	0.00	0.00	0.00	0.00	0.00	0.00	0.00	0.00	0.00	0.00
Nb ₂ O ₅	16.68	26.22	42.85	34.02	11.85	13.89	56.78	40.56	41.87	54.20	52.83
SnO ₂	0.00	0.00	0.00	0.00	0.50	0.33	0.00	0.00	0.00	0.00	0.00
Ta ₂ O ₅	64.08	53.97	35.40	46.12	69.99	67.62	21.92	37.37	38.28	24.03	24.57
WO ₃	0.40	0.25	0.24	0.24	0.44	0.36	0.00	0.27	0.43	0.00	0.61
UO ₂	0.00	0.00	0.00	0.00	0.00	0.00	0.00	0.00	0.00	0.00	0.00
Sc ₂ O ₃											
Total	99.38	99.12	98.50	99.58	100.49	100.26	98.45	99.99	99.66	98.30	98.35
Zoning	p	p	p	p	r	h (porous)	o	o	o	h	h
Formulae on basis of 6 oxygens											
Si	0.059	0.044	0.024	0.036	0.106	0.070	0.015	0.031	0.026	0.011	0.014
Al	0.000	0.000	0.000	0.000	0.000	0.006	0.000	0.000	0.000	0.000	0.000
Ti	0.043	0.032	0.023	0.025	0.051	0.044	0.023	0.023	0.023	0.014	0.021
Fe ²⁺	0.564	0.569	0.576	0.552	0.783	0.499	0.536	0.524	0.554	0.445	0.453
Mn	0.476	0.475	0.488	0.493	0.179	0.526	0.451	0.628	0.448	0.595	0.595
Mg	0.008	0.006	0.005	0.000	0.007	0.000	0.000	0.000	0.007	0.000	0.000
Zn	0.010	0.006	0.004	0.007	0.007	0.011	0.000	0.005	0.006	0.000	0.000
Ca	0.005	0.004	0.003	0.003	0.011	0.004	0.012	0.007	0.003	0.000	0.000
Nb	0.569	0.853	1.288	1.060	0.408	0.477	1.599	1.214	1.254	1.548	1.514
Ta	1.315	1.056	0.640	0.864	1.449	1.396	0.371	0.673	0.690	0.413	0.424
U	0.000	0.000	0.000	0.000	0.000	0.000	0.000	0.000	0.000	0.000	0.000
Sn	0.000	0.000	0.000	0.000	0.015	0.010	0.000	0.000	0.000	0.000	0.000
W	0.008	0.005	0.004	0.004	0.009	0.007	0.000	0.005	0.007	0.000	0.010
V	0.000	0.000	0.000	0.000	0.000	0.000	0.000	0.000	0.000	0.002	0.002
Sc											
A	1.062	1.060	1.075	1.055	1.002	1.051	0.999	1.163	1.018	1.040	1.048
B	1.986	1.986	1.974	1.985	2.014	1.986	2.008	1.940	1.994	1.987	1.974
Ta/(Ta+Nb)	0.698	0.553	0.332	0.449	0.780	0.745	0.188	0.357	0.355	0.211	0.219
Mn/(Mn+Fe)	0.457	0.455	0.458	0.472	0.186	0.513	0.457	0.545	0.447	0.572	0.568
Sample #	Polmostundra										
	3a	3b	7a	7b	7c	9a	9b	10a	10b	10c	
MgO	0.11	0.00	0.08	0.00	0.10	0.15	0.11	0.09	0.13	0.00	
Al ₂ O ₃	0.00	0.00	0.00	0.00	0.00	0.00	0.00	0.00	0.00	0.00	
SiO ₂	0.18	0.10	0.69	0.51	0.17	0.10	0.17	0.65	0.39	0.08	
CaO	0.00	0.00	0.00	0.00	0.00	0.00	0.00	0.00	0.00	0.00	
TiO ₂	0.41	1.01	0.77	0.41	0.76	0.78	0.57	1.07	0.63	0.88	
V ₂ O ₅	0.00	0.00	0.00	0.00	0.00	0.00	0.00	0.06	0.00	0.00	
MnO	4.49	6.87	4.80	5.39	3.61	4.54	5.95	6.18	4.23	4.55	
FeO	15.70	13.89	12.33	12.02	16.53	16.06	14.43	13.08	14.34	15.80	
ZnO	0.00	0.00	0.16	0.11	0.11	0.00	0.00	0.13	0.10	0.00	
ZrO ₂	0.00	0.00	0.00	0.00	0.00	0.00	0.00	0.00	0.00	0.00	
Nb ₂ O ₅	61.84	67.68	38.57	42.83	60.60	68.52	62.35	36.04	47.08	68.73	
SnO ₂	0.00	0.00	0.45	0.31	0.00	0.00	0.00	0.84	0.35	0.00	
Ta ₂ O ₅	14.90	8.90	39.75	36.11	16.76	8.22	14.55	39.17	30.12	8.13	
WO ₃	0.30	0.45	0.41	0.53	0.38	0.41	0.53	0.54	0.54	0.34	
UO ₂	0.00	0.00	0.00	0.00	0.00	0.00	0.00	0.00	0.00	0.00	
Sc ₂ O ₃											

Total	97.92	98.89	98.01	98.23	99.03	98.77	98.66	97.86	97.90	98.52
Zoning	h	h (reverse)	p	p	p	m	o	r	h	m
Formulae on basis of 6 oxygens										
Si	0.011	0.006	0.047	0.034	0.011	0.006	0.010	0.044	0.025	0.005
Al	0.000	0.000	0.000	0.000	0.000	0.000	0.000	0.000	0.000	0.000
Ti	0.019	0.044	0.039	0.021	0.035	0.034	0.026	0.055	0.031	0.039
Fe ²⁺	0.801	0.683	0.700	0.670	0.840	0.788	0.730	0.747	0.783	0.777
Mn	0.232	0.342	0.276	0.305	0.186	0.226	0.305	0.357	0.234	0.227
Mg	0.010	0.000	0.008	0.000	0.009	0.013	0.010	0.009	0.012	0.000
Zn	0.000	0.000	0.008	0.005	0.005	0.000	0.000	0.007	0.005	0.000
Ca	0.000	0.000	0.000	0.000	0.000	0.000	0.000	0.000	0.000	0.000
Nb	1.706	1.799	1.183	1.291	1.664	1.818	1.704	1.113	1.389	1.827
Ta	0.247	0.142	0.733	0.655	0.277	0.131	0.239	0.727	0.535	0.130
U	0.000	0.000	0.000	0.000	0.000	0.000	0.000	0.000	0.000	0.000
Sn	0.000	0.000	0.012	0.008	0.000	0.000	0.000	0.023	0.009	0.000
W	0.005	0.007	0.007	0.009	0.006	0.006	0.008	0.010	0.009	0.005
V	0.000	0.000	0.000	0.000	0.000	0.000	0.000	0.001	0.000	0.000
Sc	0.000	0.000	0.000	0.000	0.000	0.000	0.000	0.000	0.000	0.000
A	1.043	1.025	0.992	0.980	1.040	1.027	1.044	1.120	1.034	1.004
B	1.983	1.992	2.014	2.009	1.986	1.990	1.980	1.963	1.989	2.001
Ta/(Ta+Nb)	0.127	0.073	0.383	0.337	0.143	0.067	0.123	0.395	0.278	0.066
Mn/(Mn+Fe)	0.225	0.334	0.283	0.312	0.181	0.223	0.294	0.324	0.230	0.226
Okhmylk										
Sample #	3	4	5	6	7	13	14	15	18	19
MgO	0.00	0.00	0.00	0.00	0.00	0.00	0.00	0.00	0.00	0.00
Al ₂ O ₃	0.04	0.00	0.00	0.00	0.07	0.00	0.00	0.00	0.00	0.00
SiO ₂	0.26	0.16	0.10	0.13	0.14	0.23	0.00	0.17	0.17	0.33
CaO	0.00	0.06	0.00	0.00	0.00	0.00	0.00	0.00	0.00	0.00
TiO ₂	0.09	0.35	0.56	0.52	0.58	0.10	0.22	0.09	0.12	0.15
V ₂ O ₅	0.00	0.00	0.00	0.00	0.00	0.00	0.00	0.00	0.00	0.00
MnO	15.47	16.14	12.98	7.85	10.77	16.06	17.65	17.52	15.59	14.56
FeO	3.92	3.47	8.00	12.83	8.30	3.17	1.85	1.53	3.96	4.26
ZnO	0.00	0.02	0.00	0.00	0.00	0.00	0.00	0.00	0.00	0.00
ZrO ₂	0.00	0.00	0.00	0.00	0.00	0.00	0.00	0.00	0.00	0.00
Nb ₂ O ₅	54.44	62.17	66.94	61.59	67.03	53.70	56.61	64.37	54.26	51.93
SnO ₂	0.00	0.00	0.00	0.00	0.00	0.00	0.00	0.00	0.00	0.00
Ta ₂ O ₅	23.31	16.13	10.77	14.41	12.53	25.05	20.87	16.77	22.70	26.91
WO ₃	0.47	0.84	0.73	1.15	0.86	0.36	0.50	0.38	0.42	0.43
UO ₂	0.15	0.00	0.00	0.00	0.00					
Sc ₂ O ₃	0.00	0.15	0.16	0.18	0.23	0.11	0.14	0.08	0.10	0.14
Total	98.14	99.49	100.24	98.66	100.51	98.77	97.84	100.92	97.32	98.71
Zoning	p(rim)	p(interim)	p(core)	r	ce	p	p	p	p(core)	p(rim)
Formulae on basis of 6 oxygens										
Si	0.016	0.010	0.006	0.008	0.008	0.014	0.000	0.010	0.011	0.021
Al	0.003	0.000	0.000	0.000	0.005	0.000	0.000	0.000	0.000	0.000
Ti	0.004	0.016	0.025	0.024	0.026	0.005	0.010	0.004	0.005	0.007
Fe ²⁺	0.205	0.175	0.389	0.644	0.411	0.167	0.097	0.077	0.209	0.226
Mn	0.821	0.824	0.639	0.399	0.540	0.855	0.933	0.888	0.833	0.783
Mg	0.000	0.000	0.000	0.000	0.000	0.000	0.000	0.000	0.000	0.000
Zn	0.000	0.000	0.000	0.000	0.000	0.000	0.000	0.000	0.000	0.000
Ca	0.000	0.004	0.000	0.000	0.000	0.000	0.000	0.000	0.000	0.000
Nb	1.543	1.694	1.760	1.672	1.795	1.526	1.597	1.742	1.547	1.491
Ta	0.397	0.264	0.170	0.235	0.202	0.428	0.354	0.273	0.389	0.465
U	0.002	0.000	0.000	0.000	0.000	0.000	0.000	0.000	0.000	0.000
Sn	0.000	0.000	0.000	0.000	0.000	0.000	0.000	0.000	0.000	0.000

W	0.008	0.013	0.011	0.018	0.013	0.006	0.008	0.006	0.007	0.007
V	0.000	0.000	0.000	0.000	0.000	0.000	0.000	0.000	0.000	0.000
Sc	0.000	0.004	0.004	0.005	0.006	0.003	0.004	0.002	0.003	0.004
A	1.027	1.003	1.028	1.043	0.952	1.022	1.030	0.965	1.041	1.009
B	1.961	1.984	1.961	1.939	2.031	1.973	1.962	2.029	1.952	1.984
Ta/(Ta+Nb)	0.205	0.135	0.088	0.123	0.101	0.219	0.182	0.135	0.201	0.238
Mn/(Mn+Fe)	0.800	0.825	0.622	0.383	0.568	0.837	0.906	0.921	0.800	0.776
Shongui										
Sample #	3-1	3-2	6-1	6-2	7-1	7-2	10-1	10-2		
MgO	0.07	0.00	0.00	0.00	0.00	0.00	0.10	0.00		
Al ₂ O ₃	0.00	0.00	0.00	0.00	1.72	0.00	0.00	0.00		
SiO ₂	0.00	0.00	0.10	0.09	0.30	0.13	0.22	0.12		
CaO	0.00	0.00	0.00	0.00	0.00	0.00	0.00	0.00		
TiO ₂	2.12	1.05	0.50	0.60	0.61	0.60	1.50	1.69		
V ₂ O ₅	0.00	0.00	0.00	0.00	0.00	0.00	0.00	0.00		
MnO	6.13	6.67	8.06	7.91	10.20	7.29	6.39	8.82		
FeO	13.83	12.98	12.34	12.84	9.29	12.87	13.27	11.21		
ZnO	0.04	0.00	0.00	0.00	0.00	0.00	0.00	0.00		
ZrO ₂	0.00	0.00	0.00	0.00	0.00	0.00	0.00	0.00		
Nb ₂ O ₅	67.42	62.36	62.45	60.75	51.71	60.63	54.88	58.08		
SnO ₂	0.20	0.00	0.00	0.00	0.00	0.00	0.00	0.00		
Ta ₂ O ₅	8.04	15.53	15.04	16.21	24.96	16.84	22.49	17.64		
WO ₃	0.30	0.00	0.00	0.00	0.00	0.00	0.00	0.00		
UO ₂	0.00	0.00	0.00	0.00	0.00	0.00	0.00	0.00		
Sc ₂ O ₃	0.40	0.20	0.00	0.00	0.00	0.00	0.25	0.36		
Total	98.55	98.79	98.48	98.39	98.80	98.35	99.08	97.93		
Zoning	c	r	h	h	r	h	o	o		
Formulae on basis of 6 oxygens										
Si	0.000	0.000	0.006	0.005	0.018	0.008	0.013	0.007		
Al	0.000	0.000	0.000	0.000	0.123	0.000	0.000	0.000		
Ti	0.093	0.048	0.023	0.027	0.028	0.027	0.069	0.077		
Fe ²⁺	0.676	0.655	0.620	0.646	0.472	0.652	0.680	0.571		
Mn	0.303	0.341	0.410	0.403	0.525	0.374	0.332	0.455		
Mg	0.006	0.000	0.000	0.000	0.000	0.000	0.009	0.000		
Zn	0.002	0.000	0.000	0.000	0.000	0.000	0.000	0.000		
Ca	0.000	0.000	0.000	0.000	0.000	0.000	0.000	0.000		
Nb	1.782	1.701	1.696	1.653	1.421	1.661	1.522	1.598		
Ta	0.128	0.255	0.246	0.265	0.413	0.278	0.375	0.292		
U	0.000	0.000	0.000	0.000	0.000	0.000	0.000	0.000		
Sn	0.005	0.000	0.000	0.000	0.000	0.000	0.000	0.000		
W	0.005	0.000	0.000	0.000	0.000	0.000	0.000	0.000		
V	0.000	0.000	0.000	0.000	0.000	0.000	0.000	0.000		
Sc	0.010	0.005	0.000	0.000	0.000	0.000	0.007	0.010		
A	0.988	0.996	1.030	1.049	0.997	1.026	1.021	1.025		
B	2.008	2.004	1.970	1.951	1.879	1.974	1.979	1.975		
Ta/(Ta+Nb)	0.067	0.130	0.127	0.138	0.225	0.143	0.198	0.154		
Mn/(Mn+Fe)	0.310	0.342	0.398	0.384	0.526	0.364	0.328	0.443		

Note. p – patchy; r – overgrowing rim; o – oscillatory; h – homogeneous; m – mottled; c – core.

Table 3. Representative compositions of PSGM from the Polmostundra, Okhmylk and Shongui pegmatites.

Polmostundra										
Sample #	Pcl 1	Pcl 2	Pcl 3	Pcl 4	Pcl 5	Pcl 6	Pcl 7	Pcl 8	3-4	3-5
Na ₂ O	4.77	5.18	5.26	5.43	4.71	5.22	4.57	5.20	3.04	2.57
MgO	0.00	0.00	0.00	0.00	0.06	0.00	0.00	0.00		

Al ₂ O ₃	0.00	0.00	0.04	0.03	0.00	0.00	0.00	0.00	0.00	0.00
SiO ₂										
K ₂ O	0.00	0.00	0.00	0.00	0.00	0.00	0.00	0.00		0.25
CaO	7.73	6.17	7.78	7.52	6.98	8.28	8.63	7.09	4.47	1.95
TiO ₂	0.00	0.00	0.00	0.00	0.00	0.00	0.00	0.00		
MnO	0.00	0.00	0.11	0.00	0.22	0.00	0.14	0.17		0.18
FeO	0.00	0.00	0.00	0.00	0.00	0.00	0.00	0.00		
As ₂ O ₃										
SrO	2.78	1.76	1.09	1.36	0.88	1.15	1.29	2.01		
Y ₂ O ₃									3.04	
Nb ₂ O ₅	1.97	2.18	1.26	2.52	2.27	2.00	2.63	2.36	2.11	2.22
SnO ₂	0.00	0.28	0.30	0.81	1.13	0.34	0.66	0.55		
Ta ₂ O ₅	78.53	75.79	76.72	72.12	70.30	78.07	72.37	73.19	71.80	76.68
WO ₃	0.70	1.20	0.68	1.03	0.96	0.96	1.11	1.02	8.80	6.51
PbO	0.00	1.07	1.54	1.60	2.81	0.58	1.45	2.04	2.83	3.95
ThO ₂	0.60	0.00	0.00	0.00	0.00	0.00	0.31	0.00	0.01	0.00
UO ₂	0.00	2.55	2.25	5.80	7.24	1.02	3.51	4.58	4.84	3.37
F	2.36	1.59	1.94	1.73	1.22	2.28	1.93	2.09	0.00	
Total	99.44	97.76	98.95	99.93	98.76	99.90	98.59	100.29	100.94	97.68
O=F	0.99	0.67	0.82	0.73	0.51	0.96	0.81	0.88		
H ₂ Ocalc	0.56	0.90	0.71	0.78	0.98	0.61	0.69	0.62	1.71	1.77
Total	99.00	97.99	98.85	99.99	99.23	99.54	98.47	100.03	102.65	99.45
Formulae on basis of B=2 cations										
Na	0.825	0.913	0.937	0.986	0.876	0.899	0.828	0.940	0.518	0.423
K	0.000	0.000	0.000	0.000	0.000	0.000	0.000	0.000		0.014
Ca	0.738	0.600	0.766	0.754	0.718	0.788	0.863	0.708	0.421	0.177
Mn	0.000	0.000	0.008	0.000	0.018	0.000	0.011	0.013		0.013
Fe										
Sr	0.144	0.093	0.058	0.074	0.049	0.059	0.070	0.108		
As										
Y									0.31	
Pb	0.000	0.026	0.038	0.040	0.073	0.014	0.036	0.051	0.067	0.090
Th	0.012	0.000	0.000	0.000	0.000	0.000	0.007	0.000		
U	0.000	0.051	0.046	0.121	0.155	0.020	0.073	0.095	0.095	0.064
ΣA	1.719	1.683	1.854	1.975	1.896	1.781	1.888	1.916	1.101	0.781
Mg	0.000	0.000	0.000	0.000	0.008	0.000	0.000	0.000		
Al	0.000	0.000	0.004	0.003	0.000	0.000	0.000	0.000		
Si										
Ti	0.000	0.000	0.000	0.000	0.000	0.000	0.000	0.000		
Nb	0.079	0.089	0.052	0.107	0.098	0.080	0.111	0.099	0.084	0.085
Sn	0.000	0.010	0.011	0.030	0.043	0.012	0.025	0.021		
Ta	1.904	1.872	1.917	1.835	1.835	1.886	1.838	1.855	1.716	1.771
W	0.016	0.028	0.016	0.025	0.024	0.022	0.027	0.025	0.2	0.143
ΣB	2.000	2.000	2.000	2.000	2.000	2.000	2.000	2.000	2.000	1.999
F	0.666	0.457	0.564	0.512	0.370	0.641	0.570	0.616	0.000	0.000
OH	0.334	0.543	0.436	0.488	0.630	0.359	0.430	0.384	1.000	1.000
Vacancy	0.281	0.317	0.146	0.025	0.104	0.219	0.112	0.084	0.899	1.219
Okhmylk										
Shongui										
Sample #	10	12	10a	13	14	12a	15	16	1	2
Na ₂ O									0.62	1.55
MgO	0.00	0.00	0.00	0.00	0.00	0.00	0.00	0.00	0.08	0.10
Al ₂ O ₃	0.00	0.00	0.00	0.00	0.03	0.00	0.00	0.00	0.17	0.03
SiO ₂	0.09	0.00	0.13	0.16	0.00	0.00	0.00	0.00	5.81	6.41
K ₂ O										
CaO	15.76	15.43	14.88	15.99	15.74	15.38	15.63	15.12	16.18	15.76
TiO ₂	0.20	0.20	0.24	0.22	0.20	0.26	0.15	0.23	4.25	2.64

MnO	0.35	6.28	0.67	0.37	0.31	0.78	0.58	0.65	0.60	0.44
FeO	0.00	0.00	0.15	0.00	0.00	0.22	0.28	0.25	1.33	0.68
As ₂ O ₃									3.75	1.98
SrO										
Y ₂ O ₃			0.40	0.44	0.44	0.28	0.37	0.32		
Nb ₂ O ₅	66.90	61.54	64.58	67.09	65.74	62.21	64.52	63.18	16.27	12.02
SnO ₂	0.00	0.00							0.93	1.73
Ta ₂ O ₅	13.42	13.75	14.36	13.89	14.69	14.62	13.86	14.12	40.54	50.67
WO ₃	0.00	0.00	0.00	0.00	0.00	0.00	0.00	0.00		
PbO										
ThO ₂										
UO ₂			0.00	0.00	0.00	0.00	0.00	0.00	0.43	0.59
F	0.00	0.00	0.00	0.00	0.00	0.00	0.00	0.00	0.00	0.00
Total	96.72	97.20	95.41	98.16	97.13	93.75	95.39	93.88	90.96	94.60
O=F										
H2Ocalc	2.56	2.34	2.50	2.58	2.54	2.42	2.48	2.44	2.62	2.31
Total	99.28	99.53	97.91	100.74	99.67	96.17	97.87	96.32	93.58	96.91
Formulae on basis of B=2 cations										
Na									0.08	0.20
K										
Ca	0.989	1.043	0.955	0.995	0.995	1.021	1.014	0.995	1.149	1.096
Mn	0.018	0.335	0.034	0.018	0.015	0.041	0.030	0.034	0.034	0.024
Fe	0.000	0.000	0.007	0.000	0.000	0.011	0.014	0.013	0.074	0.037
Sr										
As									0.151	0.078
Y			0.013	0.014	0.014	0.009	0.012	0.010		
Pb									0.000	0.000
Th										
U		0.000	0.000	0.000	0.000	0.000	0.000	0.000	0.006	0.009
ΣA	1.007	1.378	1.009	1.027	1.024	1.082	1.070	1.052	1.494	1.439
Mg	0.000	0.000	0.000	0.000	0.000	0.000	0.000	0.000	0.008	0.010
Al	0.000	0.000	0.000	0.000	0.002	0.000	0.000	0.000	0.013	0.002
Si	0.005	0.000	0.008	0.009	0.000	0.000	0.000	0.000	0.525	0.567
Ti	0.009	0.009	0.011	0.010	0.009	0.012	0.007	0.011	0.212	0.129
Nb	1.772	1.755	1.748	1.762	1.754	1.742	1.765	1.754	0.487	0.353
Sn	0.000	0.000							0.025	0.045
Ta	0.214	0.236	0.234	0.219	0.236	0.246	0.228	0.236	0.730	0.894
W	0.000	0.000	0.000	0.000	0.000	0.000	0.000	0.000		
ΣB	2.000	2.000	2.001	2.000	2.001	2.000	2.000	2.001	2.000	2.000
F	0.000	0.000	0.000	0.000	0.000	0.000	0.000	0.000	0.000	0.000
OH	1.000	1.000	1.000	1.000	1.000	1.000	1.000	1.000	1.000	1.000
Vacancy	0.993	0.622	0.991	0.973	0.976	0.918	0.930	0.948	0.506	0.561

Table 4. Representative compositions of cassiterite from the Okhmylk pegmatite.

Sample #	2	3	4	5	6	7	8	9	10
MgO	0.00	0.00	0.00	0.00	0.00	0.00	0.00	0.00	0.00
Al ₂ O ₃	0.09	0.07	0.13	0.09	0.00	0.00	0.00	0.00	0.09
SiO ₂	0.27	0.26	0.28	0.27	0.18	0.29	0.26	0.31	0.29
TiO ₂	0.00	0.00	0.00	0.00	0.00	0.00	0.00	0.00	0.00
MnO	0.00	0.00	0.00	0.00	0.00	0.00	0.00	0.00	0.00
FeO	0.20	0.59	0.26	0.15	0.00	0.00	0.00	0.22	0.00
ZrO ₂	0.00	0.00	0.00	0.00	0.00	0.00	0.00	0.00	0.00
Nb ₂ O ₅	0.00	0.65	0.00	0.40	0.37	0.00	0.12	0.26	0.00
SnO ₂	98.68	94.21	97.78	98.52	98.89	99.61	99.62	98.03	98.46
Ta ₂ O ₅	0.52	3.93	1.53	0.68	0.73	0.00	0.55	0.83	0.50
WO ₃	0.00	0.00	0.00	0.00	0.00	0.00	0.00	0.00	0.00
Total	99.76	99.71	99.97	100.11	100.17	99.89	100.54	99.65	99.33

4. Results and Discussion

4.1. Zoning in CGM and included minerals

4.1.1. Kolmozero deposit

The predominant parts of the CGM grains are homogeneous or shows oscillatory zoning (sometime concentric), but some grains show irregular patchy compositional patterns (Figure 2). The oscillatory zoning observed for some CGM indicates that the grains crystallized under non-equilibrium conditions during fractional crystallization of the pegmatite melt. This compositional pattern is characteristic for magmatic CGMs from granites and pegmatites worldwide, such as the Shangbao granite [44], the Penouta leucogranite and greisen [16,45], the Separation Lake pegmatite [46], the Tanco pegmatite [11,47], the East-Qinling pegmatite district [9] and the Jezuitské Lesy pegmatite [48]. Niobium and Ta show slow diffusion relative to the rate of crystal growth in the crystallization front of the pegmatite [11,49–51], which is explained as a process of constitutional zone refining [52]. In contrast, the compositionally homogeneous CGM indicate equilibrium conditions during crystallization, with coexisting silicate melt and a separate fluid phase [53]. Under such conditions, CGM might crystallize directly from the melt.

The patchy pattern with irregularly distributed and alternating brighter and darker elongated domains (in BSE-images) throughout the CGM grains, is typical for late-stage low-temperature CGM-bearing parageneses in the Kolmozero pegmatite [8]. It has been suggested that the pattern formed during significant changes in the activities of Nb and Ta in the grain boundary fluid. The patchy pattern is somewhat similar to “myrmecitic” and “embayment” textures observed in CGM from the Chakabeishan deposit [17]. It has been suggested that these CGMs were formed by metasomatism and replacement of early-formed CGM by fluids released from the most evolved melt [46,49]. This is supported by bright overgrowths on early-formed homogeneous CGM grains, as observed in BSE-images.

Inclusions observed in the studied Kolmozero CGM include a rectangular grain of Nb-Ta-Ca-Na-oxide (30x40 μm, possibly a pyrochlore group mineral), an elongated grain of apatite (80x20 μm) and tiny (<1 μm) grains of Pb-rich uraninite, bismute, bismite, galena and sphalerite.

4.1.2. Polmostundra deposit

Although most of the CGM from the Polmostundra deposit are homogeneous, some of the grains show similar internal textures and apparently have the same origin as the Kolmozero CGM (Figure 3). Some of the grains that are homogenous and bright in BSE-images are overgrown by darker porous rims. Less abundant are patchy and mottled CGM. The patchy grains are similar to the ones from Kolmozero. Mottled (convoluted) texture is characterized by irregularly-shaped domains with embayment into each other and gradual variations in shades of gray in BSE-images. It can be observed

that the mottled texture overprints an earlier internal oscillatory zoning in grains of CGM (Figure 3 a-b). We infer that the mottled texture formed during a late stage in response to changes in the activities of Nb and Ta, in the same way as the patchy pattern. In general, CGM from the Polmostundra deposit often show reverse zoning with formation of late domains that are dark in BSE-images. This is not common for CGM from pegmatites, but it has been described from granite and pegmatite (i.e. [45,54]. Uraninite and galena are common mineral inclusions in CGM from the Polmostundra deposit.

4.1.3. Okhmylk deposit

Almost all studied CGM from Okhmylk show a patchy pattern in BSE-images, but some homogeneous grains are observed (Figure 4). The patchy pattern is represented by two subtypes: 1) alternation of dark and bright bands (Figure 4c), and 2) irregular bright domains confined to the rims of the CGM (Figure 4d). The conspicuous feature of the Okhmylk sample is the presence of abundant intergrowths of CGM and Nb-Ta-Ca-(\pm Ti, Mn)-oxide (possibly, a pyrochlore group mineral) (see section 4.3).

Subhedral Pb-rich uraninite ($<6\ \mu\text{m}$) and zircon ($<5\ \mu\text{m}$) occur as inclusions in CGM from the Okhmylk deposit, that are homogeneous in BSE-images.

4.1.4. Shongui deposit

CGM from the Shongui deposit usually exhibit a zoned texture characterized by dark-gray cores and gray rims in BSE-images (Figure 5). Occasionally this zonation is normal, and the thickness of rims is similar to the core diameter. In some cases, bright rims form thin discontinuous bands with a sharp boundary to the main crystal. These bands are inferred as late overgrowths. Some grains show oscillatory zoning, characterized by multiple bright and dark bands in BSE-images. Several grains show a complex combination of different types of zoning, such as an inner core with oscillatory zoning enclosed in a homogenous outer zone. These grains have reverse zoning, as the homogeneous outer zones are dark in BSE-images. Based on the internal textures of CGM from the Shongui deposit, the following crystallization scheme can be suggested (see previous discussion in section 4.1.1): 1) formation of oscillatory zoning during the magmatic stage under disequilibrium conditions; 2) crystallization of homogeneous CGM (dark in BSE-images) during the magmatic stage; 3) crystallization of homogeneous CGM (bright in BSE-images) from evolved melt at a late magmatic stage; 4) overgrowth of thin rims of CGM (brightest in BSE-images) at a post-magmatic (hydrothermal) stage.

Clusters of small ($<10\ \mu\text{m}$) rounded inclusions of Ta-Nb-Ca-Si-Ti-(\pm Sn)-O composition (possibly, a pyrochlore supergroup mineral) are characteristic features of CGM from the Shongui deposit. These inclusions are confined to the central parts of host mineral.

4.2. Mineral chemistry of CGM

All of the analyzed CGM from the Kolmozero-Voronja pegmatites show negative correlations in the diagrams of Nb vs. Ta and Mn vs. Fe (Figure 6a,b), suggesting the substitution of Ta with Nb and Fe with Mn. The Kolmozero CGM show highest Ta-content, while the CGM from the Okhmylk pegmatites show highest Mn-content. The Polmostundra CGM show mainly Nb- and Fe-rich compositions. Compositions and element ratios of the analyzed CGM are shown in the columbite quadrilateral diagrams (Figure 6c,d). Most of the compositions plot within the columbite-(Fe) and columbite-(Mn) fields, with single points of tantalite-(Fe), tantalite-(Mn) and species close to tapiolite-(Fe). The brightness in the domain being observed in a BSE-image of a mineral correlates with the average atomic mass of the elements constituting the domain. The atomic mass of Ta ($\approx 181\ \text{amu}$) is nearly the double of that of Nb (≈ 93), while Mn and Fe have nearly similar atomic mass ($\approx 55\ \text{amu}$ and $\approx 56\ \text{amu}$, respectively). Thus, brightest domains in the BSE images of the studied CGM grains have high Ta concentrations, while the dark domains are rich in Nb. Variations in the concentrations of Mn and Fe have much smaller effect on the brightness in BSE-images of CGM. Again, the minerals from the four studied deposits may have variable overall contents in both major (Nb, Na, Fe, Mn) and essential

minor (Ti, W, Sn, Zr, Si) components. CGM from Li pegmatites (Kolmozero, Polmostundra, Okhmylk) have impurities of Ti (0.01-0.05 apfu) and W (0.002 - 0.018 apfu), whereas mineral from Be pegmatites (Shongui) contains elevated Ti (0.02 - 0.09 apfu) and W below detection limit (Figure 7).

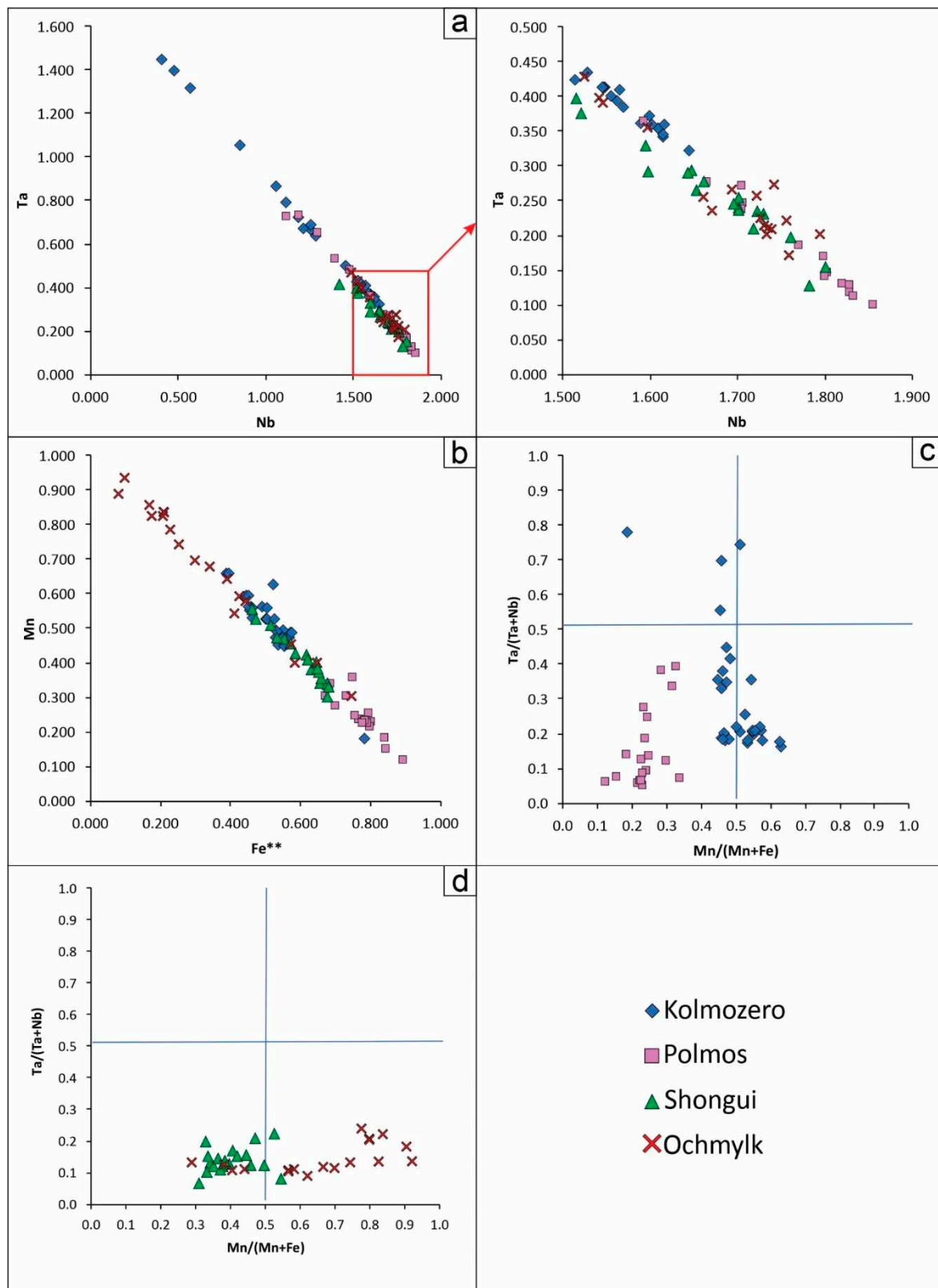


Figure 6. Major-element compositions in CGM from the Kola rare-metal pegmatite belt expressed in terms of (a) Nb (apfu) vs. Ta (apfu), (b) Mn (apfu) vs. Fe (apfu) and (c, d) Mn/(Mn + Fe) vs. Ta/(Ta + Nb).

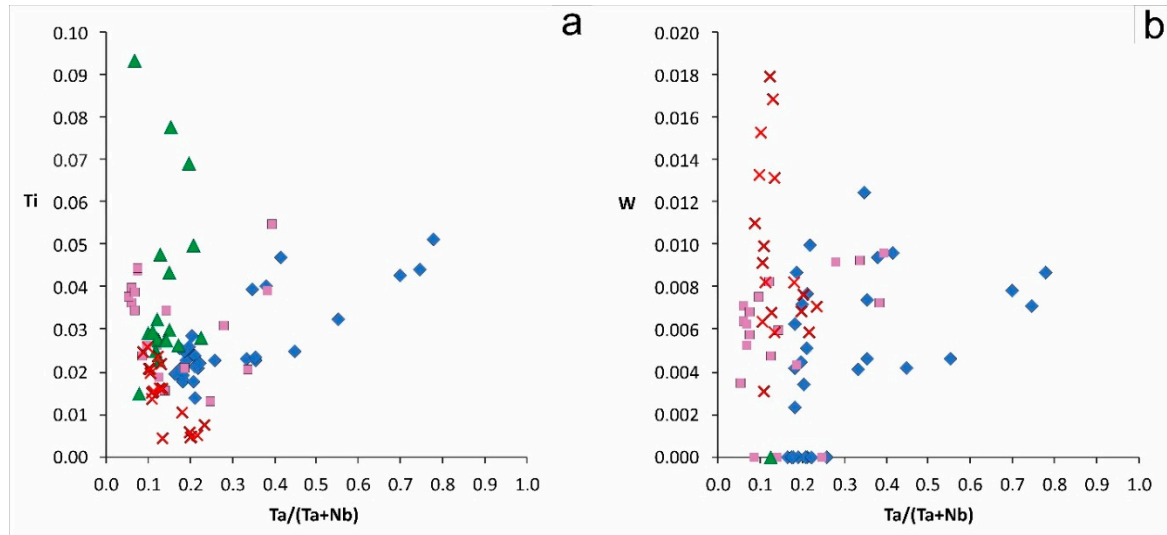


Figure 7. Minor-element compositions in CGM from the Kola rare-metal pegmatite belt expressed in terms of (a) Ta/(Ta + Nb) vs. Ti (apfu) and (b) Ta/(Ta + Nb) vs. W (apfu). Same symbols as Figure 6.

4.2.1. Kolmozero deposit

Ta/(Ta + Nb) and Mn/(Mn + Fe) ratios in Kolmozero CGM vary within 0.16–0.70 and 0.45–0.63, respectively. Most of the homogeneous CGM and CGM with oscillatory zoning are classified as columbite-(Fe) or more rare as columbite-(Mn). Most of the patchy domains in CGM classify as tantalite-(Fe) and columbite-(Mn) and rarely as columbite-(Fe). Rims and domains interpreted as late overgrowths classify as tantalite-(Fe). Some homogeneous grains of tantalite-(Mn) show a ‘sponge-like’ texture, i.e. they contain numerous tiny pores (Figure 2d). Similar textures have been related to overprinting processes resulting from influx of hydrothermal fluids (e.g. [45,55–57]). For the Kolmozero pegmatites, columbite-tantalite shows variations along two compositional trends: from columbite-(Fe) to tantalite-(Fe) and from columbite-(Fe) to columbite-(Mn) (\pm tantalite-(Mn)). This suggests a significant increase in fluorine activity during crystallization due to intensive fractionation of the pegmatite-forming melt-fluid system [19,20]. CGM from the Kolmozero deposit show low concentrations of TiO₂ (0.29 - 0.89 wt.%, average 0.54 wt.%), WO₃ (0 - 0.61 wt.%, average 0.32 wt.%) and SiO₂ (0.17 - 1.40 wt.%, average 0.39 wt.%), whereas Sn and Zr are below detection limit. High TiO₂ concentrations are observed in CGM with elevated Ta/(Ta+Nb). Patchy and porous CGM contains ZnO ranging from 0.07 to 0.20 wt.%.

4.2.2. Polmostundra deposit

The CGM from Polmostundra show compositions in the columbite-(Fe) field in Figure 5c. The Mn/(Mn + Fe) ratio varies between 0.12 and 0.33 and the Ta/(Ta + Nb) ratio between 0.05 and 0.39. The mineral shows a tendency of increasing Ta/(Ta + Nb) and in some extent of Mn/(Mn + Fe) from the homogeneous and oscillatory grains toward the patchy ones and rim overgrowths. CGM in dark zones in BSE-images with reverse zoning and embayments cutting oscillatory and homogeneous cores show lowest Ta/(Ta + Nb) in the range 0.05-0.07. The compositional variations of Nb and Ta suggest a complicated scheme for crystallization of CGM in the Polmostundra pegmatite, i.e. (1) Ta enrichment during magmatic fractionation (evidences from oscillatory and homogeneous CGM), (2) consumption of Ta in the system due to formation of other Ta-bearing minerals toward the end of the magmatic stage (outer zones in reverse CGM and embayments on mottled CGM), (3) crystallization of high-Ta CGM during a hydrothermal stage (bright domains in patchy CGM, overgrowing rims and domains). Minor components show highly variable concentrations: TiO₂ (0.27 - 1.07 wt.%, average 0.69 wt.%), WO₃ (0 - 0.54 wt.%, average 0.35 wt.%), SiO₂ (0 - 0.69 wt.%, average 0.22 wt.%), SnO₂ (0 - 0.84 wt.%, average 0.10 wt.%), and ZnO (0 - 0.16 wt.%, average 0.06 wt.%). The highest W,

Zn and Sn contents are observed from the latest CGM showing high Ta/(Ta+Nb) ratios (bright domains in patchy CGM, overgrowing rims and domains).

4.2.3. Okhmylk deposit

CGM from the Okhmylk deposit show compositions corresponding to columbite-(Fe) and columbite-(Mn) in Figure 6d, with Mn/(Mn + Fe) ratios ranging between 0.29 and 0.92, and Ta/(Ta + Nb) between 0.09 and 0.24. Some analyses with high Ta/(Ta + Nb) also show high Mn/(Mn + Fe). The highest Mn/(Mn + Fe) are detected in patchy domains (both in BSE-dark and bright domains). Homogeneous CGM and minerals with normal compositional zoning show lowest Mn/(Mn + Fe) ratios. This indicates that the enhanced Mn/(Mn + Fe) ratios result from reactions with a late hydrothermal fluid rather than during fractional crystallization (e.g., [8,11,58]). Another factor controlling the Fe-Mn fractionation in CGM is competitive crystallization of paragenetic Fe-bearing minerals (i.e. tourmaline, mica and Fe-oxides) and of Mn-bearing minerals (i.e., apatite, spessartine and triphylite-lithiophilite phosphates; see [9,59]). Abundant tourmaline (mainly schorl) together with accessory magnetite in the Okhmylk sample (see Table 1) are considered to be responsible for an increase in the Mn content of the late pegmatitic melt during continuous crystallization of CGM.

The CGM from the Okhmylk deposit differs from CGM from the other pegmatites studied here by low TiO₂ (0.09 – 0.58 wt.%, average 0.33 wt.%), high WO₃ (0.20 – 1.15 wt.%, average 0.61 wt.%), detectable Sc₂O₃ (0.08 – 0.23 wt.%, average 0.15 wt.%), and SnO₂ and ZnO below their detection limits. The minor element contents result both from melt evolution and the mineral assemblage for the Okhmylk CGM. Tungsten and Ti, as incompatible elements, prefer to enter the residual melt during magmatic evolution. Scandium is a compatible element and prefers to enter mafic minerals, such as pyroxene and amphibole. In general, pegmatites show low concentrations of Sc, but in F-enriched melts, Sc can be significantly enriched in the residual melt during magmatic evolution due to the high chemical affinity of Sc to F [60]. Absence of tin in CGM is apparently controlled by abundant cassiterite in the Okhmylk pegmatite (see Section 4.3 below).

4.2.4. Shongui deposit

The predominant CGM from the Shongui sample is columbite-(Fe) with two exceptions of columbite-(Mn). The CGM show Ta/(Ta + Nb) ratios ranging from 0.07 to 0.23 (average 0.14) and Mn/(Mn + Fe) ratios from 0.31 to 0.55 (average 0.4). Columbite-(Mn) occurs in cores that are dark in BSE-images [Ta/(Ta + Nb) = 0.08], and in overgrowths that are bright in BSE-images [Ta/(Ta + Nb) = 0.23]. The normal zoning (dark core and bright rim in BSE images) mainly reflects an increase in Ta content toward the rims. Grains with oscillatory zoning are characterized by Ta/(Ta + Nb) ratios in the range 0.15-0.2 and Mn/(Mn + Fe) ratios in the range 0.33-0.44. It may be concluded that the Nb-Ta fractionation in CGM from Shongui is mainly controlled by magmatic differentiation (both equilibrium and non-equilibrium), while hydrothermal processes (represented by rare Ta-rich overgrowing rims) are suppressed.

CGM from the Shongui deposit are characterized by minor element contents different from the other pegmatites reported here. TiO₂ ranges from 0.34 to 2.12 wt.% (average 0.84 wt.%), whereas Zr, W, Sc, Sn and Zn are negligible or below their detection limits. The highest TiO₂ content was detected in CGM with oscillatory zoning (1.5-1.7 wt.%) and in cores of grains with normal zoning (0.6-2.12 wt.%), i.e. in minerals formed during an early magmatic stage.

4.3. Associated pyrochlore supergroup minerals and cassiterite

Pyrochlore supergroup minerals (PSGM) are identified in samples from the Polmostundra, Okhmylk and Shongui pegmatites. PSGM are abundant in Polmostundra, where they form individual grains. For the Okhmylk pegmatite, PSGM occur as overgrowths on CGM, while for the Shongui pegmatite, PSGM grains occur as tiny inclusions in CGM.

PSGM from *Polmostundra* form subhedral and anhedral 200-300 µm grains (Figure 8) with an inhomogeneous internal texture characterized by irregularly distributed thin zones that are bright in

BSE images (due to high Ta, U and Pb, see Table 3). Mineral compositions are given in Table 3. The B site is mainly occupied by Ta (1.835–1.917 apfu) and, to a lesser extent, by Nb (0.052–0.111 apfu), W (0.016–0.028 apfu) and Sn (0–0.043 apfu), with Fe, Ti, Al and Mg below their detection limits. The A site is almost completely occupied by Na (0.825 to 0.986 apfu) and Ca (0.6 to 0.863 apfu), with varying contents of U (0–0.155 apfu) and Sr (0.049–0.144 apfu). The contents of Mn, Pb and Th are insignificant or below the detection limits. PSGM show variable contents of F and OH and classify as fluoronatromicrolite / hydroxynatromicrolite with an average formula $(\text{Na}_{0.90} \text{Ca}_{0.74} \text{Sr}_{0.08} \text{U}_{0.07} \text{Pb}_{0.03} \text{Mn}_{0.01})_{1.84} (\text{Ta}_{1.87} \text{Nb}_{0.09} \text{Sn}_{0.02} \text{W}_{0.02})_2 (\text{F}_{0.55} \text{OH}_{0.45})$. Microlite is the only Nb-Ta oxide from the studied pegmatite showing a significant content of uranium (1.02 to 7.24 wt. %, average 3.85 wt. %, of UO_2), suggesting that it formed during replacement of early-formed Nb-Ta minerals (i.e., [12,61]). Accordingly, the microlite shows highest Ta/(Ta + Nb) ratio (0.94–0.97) of all of the Nb and Ta oxides of the studied pegmatites, supporting its evolved character. Most analyses show fluorine >0.5 apfu, however, U-enriched microlite contains up to 0.5 apfu OH. Fluorine is below the detection limit in the thin zones with elevated Pb and U. High Pb content in microlite is partly related to secondary alteration [14]. Thus, it can be suggested that microlite crystallized during a late metasomatic / hydrothermal stage during pegmatite formation.

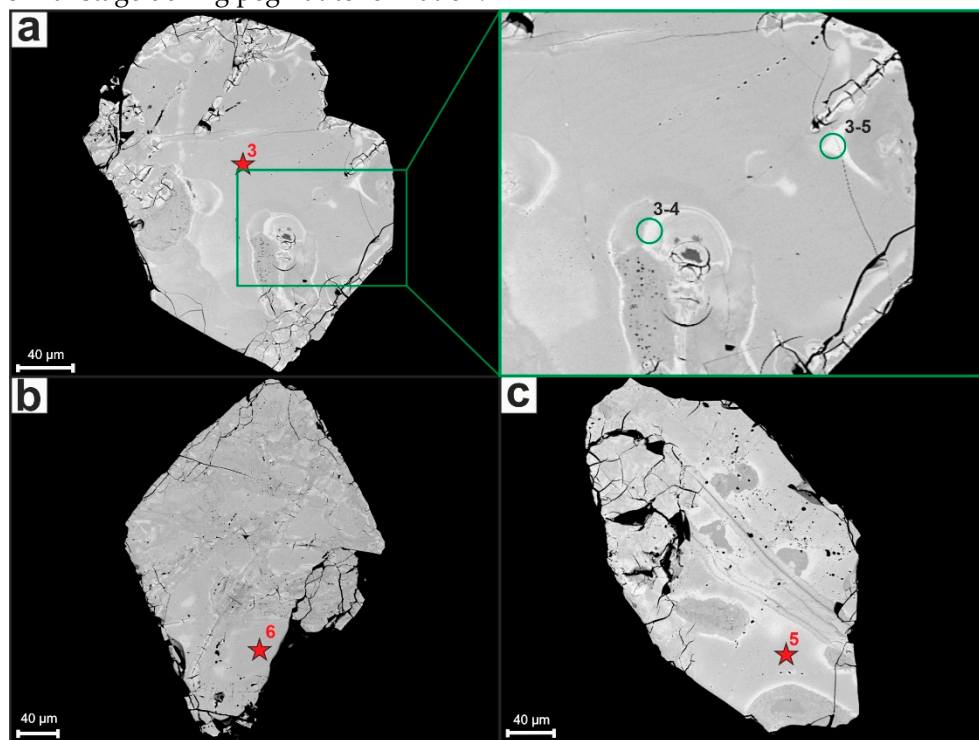


Figure 8. Representative back-scattered electron (BSE) images of PSGM grains from the Polmostudra pegmatites, illustrating the morphology and internal textures. Thin zones with elevated Ta, U and Pb (a); euhedral grains with octahedral habit (b, c). Red stars indicate microprobe analyses, green circles SEM analyses.

Okhmylk PSGM formed during replacement of columbite-(Mn). Columbite-(Mn), which formed during a magmatic stage, was initially homogeneous. The alteration of columbite-(Mn) started along the rim and internal fractures (Figure 9a) and progressed until the mineral was partly or completely altered to PSGM (Figure 9b). The PSGM from *Okhmylk* classifies as hydroxycalcipyrochlore, with the average formula $(\text{Ca}_{1.00} \text{Mn}_{0.07} \text{Fe}_{0.01} \text{Y}_{0.01})_{1.08} (\text{Nb}_{1.76} \text{Ta}_{0.23} \text{Ti}_{0.01})_2 (\text{OH}_{1.00})$. For all analyses, the contents of Na and F are below their detection limits. The mineral shows elevated Y_2O_3 content (0.28–0.44 wt. %) and high vacancies in A site (0.62–0.99 apfu). Pyrochlore and primary columbite show similar Ta/(Ta+Nb) ratios. The Mn/(Mn+Fe) ratio is exceptionally high in pyrochlore compared to columbite (0.68–1.0 and 0.57–0.67, correspondingly). The replacement process was probably driven by Ca-rich hydrothermal solutions. During the alteration, both Nb and Ta appear to have been immobile. The Mn-Fe substitution series shows the fractionation with removal of iron.

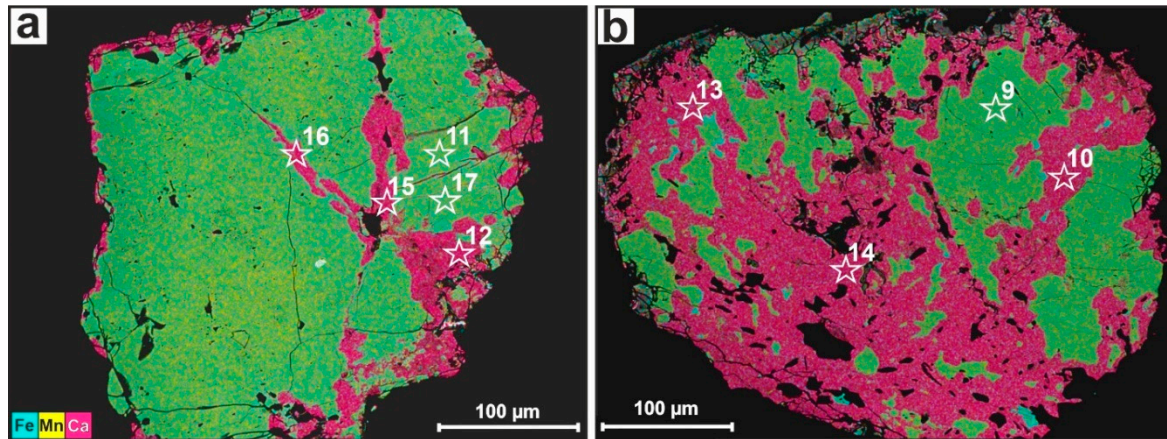


Figure 9. EMPA mapping (Fe, Mn, Ca) of CGM and PSGM showing the formation of PSGM along the rim and internal fractures in CGM (a), and more extensive replacement of CGM by PSGM (b). Stars indicate microprobe analyses.

An estimate of the average composition of *PSGM* from *Schongui* (see Figure 5d) suggests that the mineral is hydroxycalciummicrolite with the formula $(\text{Ca}_{1.13} \text{Na}_{0.12} \text{As}_{0.07} \text{Fe}_{0.06} \text{Mn}_{0.03} \text{U}_{0.02})_{1.42} (\text{Ta}_{0.91} \text{Si}_{0.65} \text{Nb}_{0.37} \text{Sn}_{0.04} \text{Mg}_{0.01} \text{Al}_{0.01})_2 (\text{OH}_{1.00})$. The average $\text{Ta}/(\text{Ta}+\text{Nb})$ and $\text{Mn}/(\text{Mn}+\text{Fe})$ are 0.72 and 0.38, respectively. The host mineral is columbite-(Fe) or, less common, columbite-(Mn), with $\text{Ta}/(\text{Ta}+\text{Nb})$ and $\text{Mn}/(\text{Mn}+\text{Fe})$ ratios in the range 0.08-0.17 and 0.41-0.54, respectively.

Cassiterite was recovered only from the Okhmylk pegmatite. The mineral occurs as anhedral and subhedral angular grains (200-300 µm) (Figure 10). The internal texture is inhomogeneous due to the presence of porous domains. Cassiterite grains often contain inclusions (20-40 µm) of albite and rarely quartz, resembling a poikilitic texture. These textural patterns are different from those observed in cassiterites forming at magmatic stages of pegmatite formation (i.e. homogeneous, without pores and inclusions of late minerals, see [46,58,62]). Cassiterite contains inclusions of rounded and partially resorbed CGM (40-60 µm). The CGM are of both magmatic (normal compositional zoning) and metasomatic/hydrothermal (with patchy domains) types. Cassiterite, enclosing magmatic CGM, has been reported from a number of pegmatite occurrences, i.e. Separation Rapids in Canada [46] and Kangxiwa–Dahongliutan in China [58]. The chemical composition of cassiterite from Okhmylk is near ideal SnO_2 (the majority of the grains have > 99 wt. % SnO_2) with variable contents of trace elements (Fe: 0 – 0.012, average 0.003 apfu; Nb: 0 – 0.007, average 0.002 apfu; Ta: 0 – 0.027, average 0.007 apfu; Mn, Mg, Zr, Ti are below their detection limits). The compositions are typical for cassiterite from hydrothermal environment [62].

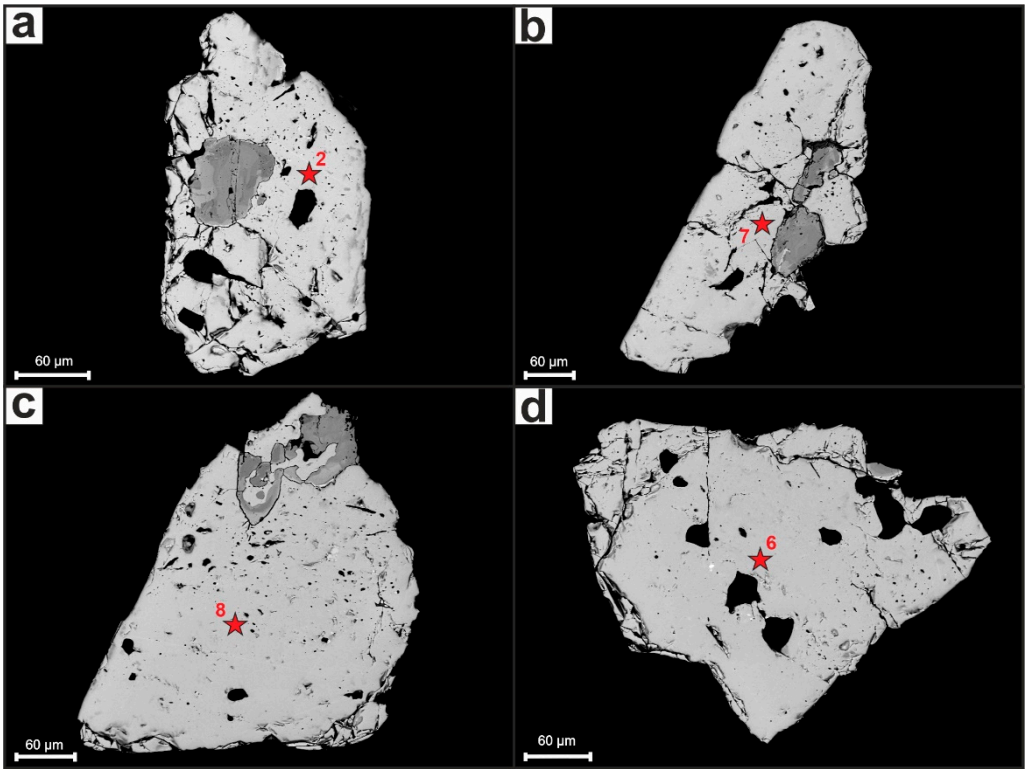


Figure 10. Representative back-scattered electron (BSE) images of cassiterite grains from the Okhmylk pegmatites, showing morphology and internal textures. Inclusions of CGM (a, b, c); porous texture and rounded inclusions of quartz and albite (a, b, c, d).

4.4. Implication for ore genesis and grade

Nb-Ta-Sn oxides (among which the columbite group minerals, the pyrochlore supergroup minerals and cassiterite are the most common) can provide information about the formation of LCT-pegmatites of different ore grades and mineralization signatures. Variations in the composition and internal textures of Nb-Ta-Sn oxides are mainly controlled by the rate of magmatic fractionation, mineral associations of the host pegmatite, the composition of the magmatic fluid, and later hydrothermal/metasomatic processes. As a result of fractional crystallization, the composition of CGM generally shows a continuum from early Nb-rich to later Ta-rich compositions [63,64]. Normal and oscillatory zoning, homogeneous compositions are of magmatic origin and controlled by Nb-Ta fractionation. Previous studies have proved that the patchy and mottled textures of CGM, as well as overgrowing Ta-rich rims, are generally related to metasomatic replacement during reactions with hydrothermal fluids (e.g., [8,11,58]). Fractionation of Fe and Mn, which is difficult to relate to any of the processes mentioned above, was probably controlled by the mineral associations during crystallization. Reverse zoning is rarely observed in CGM from rare-metal pegmatites and may be attributed to local changes of the bulk geochemistry and/or fluid regime of the pegmatite.

The main compositional and textural features of Nb-Ta-Sn oxides from the studied pegmatite samples from the Kolmozero-Voronja belt are summarized in Table 5.

Table 5. Summary of mineralogical studies of Nb-Ta-Sn oxides from pegmatite samples in Kolmozero-Voronja rare-metal belt.

Deposit/Occurrence	Kolmozero	Polmostundra	Okhmylk	Shongui
Sample N	KL-GX-11	POL-GX-3/5	OKH-2/2	SH-7
Mineralization signature	Li (±Nb, Ta)	Li-Cs (±Nb, Ta)	Li (±Nb, Ta)	Be (±Nb, Ta)
Ore grade (based on Li content)	High	Medium to low	Low to barren	Low to barren

CGM	columbite-(Fe) columbite-(Mn) tantalite-(Fe) tantalite-(Mn)	columbite-(Fe)	columbite-(Fe) columbite-(Mn)	columbite-(Fe) columbite-(Mn)
Texture/zoning/ pattern (by descending)	oscillatory homogeneous patchy sponge domains overgrowing Ta- rich rims	homogeneous mottled oscillatory patchy irregular reverse	irregular normal patchy homogeneous	progressive normal oscillatory homogeneous irregular reverse overgrowing Ta-rich rims
Overall composition features:				
Ta/(Ta + Nb)	0.16–0.70	0.05–0.39	0.09–0.24	0.07–0.23
Mn/(Mn + Fe)	0.45–0.63	0.12–0.33	0.29–0.92	0.31–0.55
Ti (apfu)	0.01–0.05	0.01–0.05	0–0.025	0.02–0.09
W (apfu)	0.002–0.012	0.0–0.009	0.003–0.018	0.0
PSGM	calciopyrochlore (included into columbite-(Fe))	fluoronatromicrolite (abundant individual grains of hydrothermal origin)	hydroxycalcipyrochlore (replaced columbite- (Mn))	hydroxycalciumicrolite (included into columbite-(Fe))
Cassiterite	No (0–0.5 wt.% of SnO ₂ in CGM)	No (0–0.84 wt.% of SnO ₂ in CGM)	abundant porous grains of hydrothermal origin (0.0 wt.% of SnO ₂ in CGM)	No (0–0.2 wt.% of SnO ₂ in CGM)
Main evolution trends for Nb-Ta-Sn oxides:	Calciopyrochlore → columbite-(Fe) → columbite- (Mn); columbite- (Fe) → tantalite- (Fe)/tantalite- (Mn).	Columbite-(Fe) → columbite-(Fe) with higher Ta/(Ta+Nb) → fluornatromicrolite → hydroxynatromicrolite with high Ta, U and Pb content.	Columbite-(Fe)/ columbite-(Mn) → hydroxycalcipyrochlore → cassiterite.	Hydroxycalciumicrolite → columbite-(Fe) → columbite-(Fe) with higher Ta/(Ta+Nb).

Based on the information given in Table 5 we infer that both magmatic and hydrothermal processes controlled the Nb-Ta and Fe-Mn fractionation of CGM from the high grade Kolmozero Li deposit. For the medium- to low-grade Polmostundra Li (\pm Cs) deposit, magmatic processes were less pronounced for Nb-Ta fractionation of the CGM, while hydrothermal processes were important during crystallization of microlite. For the low-grade Okhmylk Li deposit we infer that Nb-Ta fractionation was insignificant for CGM during the magmatic stage. However, the fractionation of Fe and Mn controlled by the mineral association, i.e. the crystallization of Fe minerals (schorl) was significant in Okhmylk CGM. Hydroxycalcipyrochlore and cassiterite are of hydrothermal origin. For the CGM from the low-grade Shongui Be (\pm Ta) deposit, any Nb-Ta fractionation during magmatic stage is considered to be insignificant. The hydroxycalcio- species of PSGM crystallized during an early magmatic stage, while the fluoronatro- species formed in hydrothermal environment, probably during reactions with sodium and fluorine in excess in late hydrothermal solutions.

Late tantalum-rich Nb-Ta oxides (CGM and PSGM from Kolmozero and Polmostundra) have elevated Sn content that is in accordance with presumable partitioning of tin into late hydrothermal phases [65]. The consumption of Sn by abundant CGM from these deposits did not allow cassiterite precipitation. The opposite can be inferred for the niobium-rich CGM and PSGM from Okhmylk, which do not contain Sn. Here, Sn was allowed to accumulate in the late fluid phase, resulting in the crystallization of hydrothermal cassiterite.

The petrogenetic processes that were active during the formation of the high-grade Kolmozero deposit, resulted in the crystallization of abundant CGM, showing large compositional variations. Volatile components may have played an important role for the rare-metal enrichment. Indeed, the

Kolmozero sample has an elevated concentration of CO₂ (0.25 wt.% vs <0.01-0.02 wt.% in low-grade samples (see Table 1). Due to the strong depolymerization effect of CO₂, a high CO₂ content causes rapid separation of volatile-rich melts from the initial magma through immiscibility [66]. At this stage, the activity of rare metals increased. Furthermore, CO₂ is exhausted earlier than other volatiles, promoting extensive hydrothermal processes and rare metal precipitation, in response to pressure and temperature drop and/or pH change [67].

5. Conclusions

1. CGM from high-grade Li pegmatite deposits from the Kolmozero-Voronja belt are characterized by several mineral species showing large variations in chemical compositions, mainly controlled by Nb-Ta fractionation. Textural patterns are extremely various and indicate the involvement of numerous magmatic and hydrothermal processes.
2. Nb-Ta magmatic fractionation in CGM from low-grade and barren pegmatite deposits is insignificant.
3. Fe-Mn fractionation is mainly controlled by precipitation of certain Fe minerals during pegmatite formation and does not play an important role in the grade of the deposits.
4. PSGM from high- to medium-grade lithium deposits are magmatic (Nb varieties) and early hydrothermal (Ta varieties), while in low-grade to barren pegmatites the mineral crystallized at late hydrothermal stages (both Nb and Ta varieties). PSGM from beryllium deposits are early magmatic Ta varieties and crystallized before CGM.
5. Sn is concentrated in CGM from high- to medium-grade Li pegmatites, while it formed abundant hydrothermal cassiterite in low-grade and barren pegmatites.
6. Be-Ta pegmatites from the Kolmozero-Voronja belt are characterized by CGM with lowest variations of fractionation ratios Ta/(Ta + Nb) and Mn/(Mn + Fe) and highest Ti contents.

Supplementary Materials: The following supporting information can be downloaded at the website of this paper posted on Preprints.org.

Acknowledgments: The research has been carried out in the framework of the Russian Science Foundation Grant No. 22-17-20002, <https://rscf.ru/project/22-17-20002/> (accessed on 25 March 2022). We thank S. Mudruk and A. Solovjeva, who assisted with drawing, and T. Zikova for Nb-Ta-Sn oxides separation.

References

1. Černý, P., Ercit, T.S., 1985. Some recent advances in the mineralogy and geochemistry of Nb and Ta in rare-element granitic pegmatites. *Bulletin of Mineralogy* 108, 499–532.
2. Černý, P., Ercit, T.S., 1989. Mineralogy of niobium and tantalum: crystal chemical relationships, paragenetic aspects and their economic implications. In: Moller, P., Cerny, P., Saupe, F. (Eds.), *Lanthanides, Tantalum and Niobium*. Springer Verlag, Heidelberg, pp. 27–79.
3. Raimbault, L., 1998. Composition of complex lepidolite-type granitic pegmatites and of constituent columbite-tantalite, Chedeville, Massif Central, France. *The Canadian Mineralogist* 36, 563–583.
4. Uher, P., Černý, P., Chapman, R., Hatar, J., Miko, O., 1998. Evolution of Nb-Ta-oxide minerals in the Prasiva granitic pegmatites, Slovakia; I, Primary Fe, Ti-rich assemblage. *The Canadian Mineralogist* 36, 525–534.
5. Lumpkin G.R., 1998. Composition and Structural State of Columbite - Tantalite from the Harding Pegmatite, Taos County, New Mexico. *The Canadian Mineralogist* 36, 585–599.
6. Novák, M., Uher, P., Černý, P., Šiman, P., 2000. Compositional variations in ferrotapiolite+tantalite pairs from the beryl-columbite pegmatite at Moravany nad Váhom, Slovakia. *Mineralogy and Petrology* 69, 295–306.
7. Beurlen, H., Da Silva, M.R.R., Thomas, R., Soares, D.R., Olivier, P., 2008. Nb-Ta-(Ti-Sn) oxide mineral chemistry as tracer of rare-element granitic pegmatite fractionation in the Borborema Province, Northeastern Brazil. *Mineral Deposits* 43, 207–228. <http://doi.org/10.1007/s00126-007-0152-4>.
8. Badanina, E.V., Sitnikova, M.A., Gordienko, V.V., Melcher, F., Gäbler, H.E., Lodziak, J., Syritso, L.F., 2015. Mineral chemistry of columbite-tantalite from spodumene pegmatites of Kolmozero, Kola Peninsula (Russia). *Ore Geology Reviews* 64, 720–735. [CrossRef]
9. Zhou, Q., Qin, K., Tang, D., 2021. Mineralogy of columbite-group minerals from the rare-element pegmatite dykes in the East-Qinling orogen, central China: Implications for formation times and ore genesis. *Journal of Asian Earth Sciences* 218, 104879. <https://doi.org/10.1016/j.jseas.2021.104879>.

10. Zhang, A.C., Wang, R.C., Hu, H., Zhang, H., Zhu, J.C., Chen, X.M., 2004. Chemical evolution of Nb-Ta oxides and zircon from the Koktokay No.3 granitic pegmatite, Altai, northwestern China. *Mineralogical Magazine* 68, 739–756.
11. van Lichtervelde, M., Salvi, S., Beziat, D., Linnen, R.L., 2007. Textural features and chemical evolution in tantalum oxides: Magmatic versus hydrothermal origins for Ta mineralization in the Tanco Lower Pegmatite, Manitoba, Canada. *Economic Geology* 102, 257–276.
12. Llorens, T., Moro, M.C., 2010. Microlite and Tantalite in the LCT Granitic Pegmatites of La Canalita, Navasfrías Sn–W District, Salamanca, Spain. *The Canadian Mineralogist* 48, 375–390. <https://doi.org/10.3749/canmin.48.2.375>.
13. Martins, T., Lima, A., Simmons, W.B., Falster, A.U., Noronha, F., 2011. Geochemical fractionation of Nb-Ta oxides in Li-bearing pegmatites from the Barroso-Alvão pegmatite field, northern Portugal. *The Canadian Mineralogist* 49, 777–791.
14. Melcher, F., Graupner, T., Gäbler, H.-E., Sitnikova, M., Henjes-Kunst, F., Oberthür, T., Gerdes, A., Dewaele, S., 2015. Tantalum–(niobium–tin) mineralisation in African pegmatites and rare metal granites: Constraints from Ta–Nb oxide mineralogy, geochemistry and U–Pb geochronology. *Ore Geology Reviews* 64, 667–719. <https://doi.org/10.1016/j.oregeorev.2013.09.003>
15. Melcher, F., Graupner, T., Gäbler, H.-E., Sitnikova, M., Oberthür, T., Gerdes, A., Badanina, E., Chudy, T., 2017. Mineralogical and chemical evolution of tantalum–(niobium–tin) mineralisation in pegmatites and granites. Part 2: Worldwide examples (excluding Africa) and an overview of global metallogenetic patterns. *Ore Geology Reviews* 89, 946–987.
16. González, T.L., Polonio, F.G., Moro, F.J.L., Fernández, A.F., Contreras, J.L.S., Benito, M.C.M., 2017. Tin-tantalum-niobium mineralization in the Penouta deposit (NW Spain): Textural features and mineral chemistry to unravel the genesis and evolution of cassiterite and columbite group minerals in a peraluminous system. *Ore Geology Reviews* 81, 79–95.
17. Sun, W., Zhao, Z., Mo, X., Wei, C., Dong, G., Li, X., Yuan, W., Wang, T., Yang, S., Wang, B., Pan, T., Han, J., Cao, H., Tang, Y., Zhang, L., 2023. Age and Composition of Columbite-Tantalite Group Minerals in the Spodumene Pegmatite from the Chakabeishan Deposit, Northern Tibetan Plateau and Their Implications. *Minerals* 13, 201. <https://doi.org/10.3390/min13020201>.
18. Černý, P., 1989. Characteristics of pegmatite deposits of tantalum. In: Möller, P., Černý, P., Saupé, F. (Eds.), *Lanthanides, Tantalum and Niobium*. Springer-Verlag, Berlin, pp. 195–239.
19. Spilde, M.N., Shearer, C.K., 1992. A comparison of tantalum - niobium oxide assemblages in two mineralogically distinct rare-element granitic pegmatites, Black Hills, South Dakota. *The Canadian Mineralogist* 30, 719–737.
20. Černý, P., Němec, D., 1995. Pristine vs. contaminated trends in Nb,Ta-oxide minerals of the Jihlava pegmatite district, Czech Republic. *Mineralogy and Petrology* 55, 117–129.
21. Linnen, R.L., van Lichtervelde, M., Černý, P., 2012. Granitic pegmatites as sources of strategic metals. *Elements* 8, 275–280.
22. Multimedia reference book on mineral resources and the mining complex of the Murmansk region: a digital information resource, 2001. Mitrofanov F.P., Lebedev A.V. (Eds), GI KSC RAS, Apatity. (in Russian)
23. Mints, M.V., Dokukina, K.A., Filippova, I.B., Konilov, A.N., 2015. East European Craton: Early Precambrian History and 3D Models of the Deep Structure of the Earth's Crust. Geological Society of America (GSA), Boulder, Colorado, 433 pp.
24. Daly, J.S., Balagansky, V.V., Timmerman, M.J., Whitehouse, M.J., 2006. The Lapland-Kola Orogen: Palaeoproterozoic collision and accretion of the northern Fennoscandian lithosphere. In: Gee D.G., Stephenson R.A. (Eds), *European Lithosphere Dynamics, Memoir 32*. Geological Society, London, pp. 579–597.
25. Belolipetsky, A.P., Gaskelberg, V.G., Gaskelberg, L.A., Antonyuk, E.S., Ilyin, Yu.I., 1980. Geology and geochemistry of metamorphic complexes of the Early Precambrian of the Kola Peninsula. L.: Science, 240 pp. (in Russian)
26. Vrevsky, A.B., 1989. Petrology and geodynamic modes of development of the Archean lithosphere (on the example of the northeastern part of the Baltic Shield). L.: Science, 143 pp. (in Russian)
27. Glebovitsky V.A. Early Precambrian of the Baltic Shield, 2005. Science, St. Petersburg, 711 pp. (in Russian)
28. Hölttä, P., Balagansky, V., Garde, A.A., Mertanen, S., Peltonen, P., Slabunov, A., Sorjonen-Ward, P., Whitehouse, M., 2008. Archean of Greenland and Fennoscandia. *Episodes* 31, 13–19.
29. McCaffrey, K.J.W., Lonergan, L., Wilkinson, J.J. Fractures. Fluid Flow and Mineralization. Geological Society of London. London, 337 pp.
30. Morozova, L.N., 2018. Kolmozero lithium deposit of rare metal pegmatites: new data on rare element composition (Kola Peninsula). *Lithosphere* 18, 82–98. <https://doi.org/10.24930/1681-9004-2018-18-1-082-098>.
31. Morozova, L.N., Bazai, A.V., 2019. Spodumene from rare-metal pegmatites of the Kolmozerskoe lithium deposit (Kola Peninsula). *Proceedings of the Russian Mineralogical Society* 148 (1), 65–78. (in Russian)

32. Morozova, L.N., Sokolova, E.N., Smirnov, S.Z., Balagansky, V.V., Bazai, A.V., 2021. Spodumene from rare-metal pegmatites of the Kolmozero lithium world-class deposit on the Fennoscandian shield: trace elements and crystal-rich fluid inclusions. *Mineralogical Magazine* 85 (2), №557, 149-160.
33. Zozulya, D., Macdonald, R., Bagiński, B., 2020. REE fractionation during crystallization and alteration of fergusonite-(Y) from Zr-REE-Nb-rich late- to post-magmatic products of the Keivy alkali granite complex, NW Russia. *Ore Geology Reviews* 125, 103693. <https://doi.org/10.1016/j.oregeorev.2020.103693>.
34. Gordienko, V. V., 1970. Mineralogy, geochemistry and genesis of spodumene pegmatites. L.: Nedra, 239 pp. (in Russian)
35. Morozova, L.N., Bayanova, T.B., Bazai, A.V., Lyalina, L.M., Serov, P.A., Borisenko, E.S., Kunakkuzin, E.L., 2017. Rare-metal pegmatites of the Kolmozerskoe lithium deposit in the Arctic region of the Baltic Shield: new geochronological data. *Bulletin of the Kola Science Center of the Russian Academy of Sciences*, 1, 43–52. (in Russian)
36. Hanski, E.J., Melezhik, V.A., 2013. Litho- and chronostratigraphy of the Palaeoproterozoic Karelian formations. In: Melezhik V.A. (Ed), *Reading the Archive of Earth's Oxygenation*, v. 2. Springer, Berlin, pp. 39–110
37. Kudryashov, N.M., Udoratina, O.V., Kalinin, A.A., Lyalina, L.M., Selivanova, E.A., Grove, M.J., 2022. U-Pb (SHRIMP-RG) age of zircon from rare-metal (Li, Cs) pegmatites of the Okhmylk deposit of the Kolmozero-Voron'ya greenstone belt (northeast of the Fennoscandian shield). *Journal of Mining Institute* 255, 448-454. <https://doi.org/10.31897/PMI.2022.41>.
38. Antonyuk, E.S., 1962. Structural-mineral complexes of granite pegmatite veins, Materials on the mineralogy of the Kola Peninsula. KFAN USSR, Apatity, pp. 134-142. (in Russian)
39. Polkanov, A.A., Gerling, E.K., 1961. Geochronology and geological evolution of the Baltic Shield and its folded framing. *Trudy LAGED* 12, 101-102. (in Russian)
40. Černý, P., Ercit, S., 2005. The classification of granitic pegmatites revisited. *The Canadian Mineralogist* 43, 2005-2026. <http://doi.org/10.2113/gscanmin.43.6.2005>.
41. Müller, A., Romer, R.L., Pedersen, R.B. 2017. The Sveconorwegian pegmatite province – Thousands of pegmatites without parental granites. *The Canadian Mineralogist* 55, 283–315.
42. Webber, K.L., Simmons, W.B., Falster, A.U., Hanson, S.L. 2019. Anatectic pegmatites of the Oxford County pegmatite field, Maine, USA. *The Canadian Mineralogist* 57, 811–815.
43. Silva, D., Groat, L., Martins, T., Linnen, R. 2023. Structural controls on the origin and emplacement of lithium-bearing pegmatites. *The Canadian Journal of Mineralogy and Petrology* 61, <https://doi.org/10.3749/2300045>
44. Zhao, Z., Yang, X., Lu, S., Lu, Y., Sun, C., Chen, S., Chen, S.S., Zhang, Z.Z., Bute, S.I., Zhao, L.L., 2021. Genesis of Late Cretaceous granite and its related Nb-Ta-W mineralization in Shangbao. Nanling Range: Insights from geochemistry of whole-rock and Nb-Ta minerals. *Ore Geology Reviews* 131, 103975.
45. Alfonso, P., Hamid, S., Garcia-Valles, M., Llorens, T., López Moro, F., Tomasa, O., Calvo, D., Guasch, E., Anticoi, H., Oliva, J., Parcerisa, D., García, Polonio F., 2018. Textural and mineral-chemistry constraints on columbite-group minerals in the Penouta deposit: Evidence from magmatic and fluid-related processes. *Mineralogical Magazine* 82 (S1), 199-222. <https://doi.org/10.1180/minmag.2017.081.107>.
46. Tindle, A.G., Breaks, F.W., 2000. Columbite-tantalite mineral chemistry from rare-element granitic pegmatites: Separation Lakeh area, NW Ontario. Canada. *Mineralogy and Petrology* 70, 165–198.
47. Černý, P., 2005. The Tanco rare-element pegmatite deposit, Manitoba: regional context, internal anatomy, and global comparisons. In: Linnen, R.L., Samson, I.M. (Eds.), *Rare-Element Geochemistry and Mineral Deposits*. Geological Association of Canada, GAC Short Course Notes, vol. 17, pp. 127–158.
48. Chudík, P., Uher, P., Gadas, P., Škoda, R., Pršek, J., 2011. Niobium-tantalum oxide minerals in the Jezuitské Lesy granitic pegmatite, Bratislava Massif, Slovakia: Ta to Nb and Fe to Mn evolutionary trends in a narrow Be, Cs-rich and Li, B-poor dike. *Mineralogy and Petrology* 102, 15–27.
49. Lahti, S.I., 1987. Zoning in columbite-tantalite crystals from the granitic pegmatites of the Eräjärvi area, southern Finland. *Geochimica et Cosmochimica Acta* 51, 509–517.
50. van Lichtenvelde, M., Linnen, R.L., Salvi, S., Beziat, D., 2006. The role of metagabbro rafts on tantalum mineralization in the Tanco granitic pegmatite, Manitoba. *The Canadian Mineralogist*. 44, 625–644.
51. van Lichtenvelde, M., Holtz, F., Melcher, F., 2018. The effect of disequilibrium crystallization on Nb-Ta fractionation: Constraints from crystallization experiments of tantalite-tapiolite. *American Mineralogist* 103, 1401–1416.
52. London, D., 2018. Ore-forming processes within granitic pegmatites. *Ore Geology Reviews* 101, 349–383.
53. Jahns, R.H., Burnham, C.W., 1969. Experimental studies of pegmatite genesis: I, A model for the derivation and crystallization of granitic pegmatites. *Economic Geology* 64, 843–864.
54. Novák, M., Černý, P., Uher, P., 2003. Extreme variation and apparent reversal of Nb-Ta fractionation in columbite-group minerals from the Scheibengraben beryl-columbite granitic pegmatite, Maršíkov, Czech Republic. *European Journal of Mineralogy* 15, 565 – 574.

55. Galliski, M.A., Márquez-Zavalía, M.F., Černý, P., Martínez, V.A., Capman, R., 2008. The Ta-Nb-Sn-Ti oxide mineral paragenesis from La Viquita, a spodumene bearing rare-element granitic pegmatite, San Luis, Argentina. *The Canadian Mineralogist* 30, 379–393.
56. Wise, M.A., Brown, C.D., 2010. Mineral chemistry, petrology and geochemistry of the Sebago granite-pegmatite system, southern Maine, USA. *Journal of Geosciences* 55, 3–26.
57. Zhu, Z.Y., Wang, R.C., Che, X.D., Zhu, J.C., Wei, X.L., Huang, X., 2015. Magmatic-hydrothermal rare element mineralization in the Songshugang granite (northeastern Jiangxi, China): Insights from an electron-microprobe study of Nb-Ta-Zr minerals. *Ore Geology Reviews* 65, 749–760.
58. Feng, Y.G., Liang, T., Yang, X.Q., Zhang, Z., Wang, Y.Q., 2019. Chemical evolution of Nb-Ta Oxides and Cassiterite in phosphorus-rich albite-spodumene pegmatites in the Kangxiwa-Dahongliutan pegmatite field, Western Kunlun Orogen, China. *Minerals* 9 (166), 1–39.
59. Duan Z.-P., Jiang S.-Y., Su H.-M., Zhu X.Y., Zou T., 2022. Nb-Ta oxides as recorders of hydrothermal activity in the Shihuiyao Rb-Nb-Ta-(Be-Li) deposit, Inner Mongolia, NE China. *Ore Geology Reviews* 150, 105149
60. Shchekina, T.I., Gramenitskii, E.N., 2008. Geochemistry of Sc in the magmatic process: experimental evidence. *Geochemistry International* 46 (4), 351–366.
61. Von Knorring, O., Fadipe, A., 1981. On the mineralogy and geochemistry of niobium and tantalum in some granite pegmatites and alkali granites of Africa. *Bulletin of Mineralogy* 104, 496–507.
62. Breiter, K., Skoda, R., Uher, P., 2007. Nb-Ta-Ti-W-Sn-oxide minerals as indicators of a peraluminous P- and F-rich granitic system evolution: Podlesí, Czech Republic. *Mineralogy and Petrology* 91, 225–248.
63. Linnen, R.L., Keppler, H., 1997. Columbite solubility in granitic melts: consequences for the enrichment and fractionation of Nb and Ta in the Earth's crust. *Contrib. Mineral. Petrol.* 128, 213–227.
64. Fiege, A., Kirchner, C., Holtz, F., Linnen, R.L., Dziony, W., 2011. Influence of fluorine on the solubility of manganotantalite (MnTa₂O₆) and manganocolumbite (MnNb₂O₆) in granitic melts – an experimental study. *Lithos* 122, 165–174.
65. Kaeter, D., Barros, R., Menuge, J.F. 2021. Metasomatic High Field Strength Element, Tin, and Base Metal Enrichment Processes in Lithium Pegmatites from Southeast Ireland. *Economic Geology* 116 (1), 169–198. <https://doi.org/10.5382/econgeo.4784>
66. Zhang, D.H., Zhang, W.H., Xu, G.J., 2004. The ore fluid geochemistry of F-rich silicate melt-hydrous fluid system and its metallogeny-the current status and problems. *Earth Science Frontiers* 11, 479–490.
67. Seward, T.M., Barnes, H.L., 1997. Metal transport by hydrothermal ore fluids. *Geochem. Hydrothermal Ore Depos.* 3, 435–486.

Disclaimer/Publisher's Note: The statements, opinions and data contained in all publications are solely those of the individual author(s) and contributor(s) and not of MDPI and/or the editor(s). MDPI and/or the editor(s) disclaim responsibility for any injury to people or property resulting from any ideas, methods, instructions or products referred to in the content.